Chapter 3

Magnetic Properties of CoTbNi Ternary Alloy Thin Film

Chapter 3

Magnetic Properties of CoTbNi Ternary Alloy Thin Film

In this chapter, the magnetic properties of CoTbNi ternary alloy thin films prepared under two deposition conditions are discussed. The details of four measurement results namely compositional analysis by SEM-EDS, film surface topography, and roughness measurement by 3D optical profilometer, crystal structural analysis by X-ray diffraction technique and magnetic properties measurement by vibrating sample magnetometer have been discussed in the current chapter. The detail of the sample fabrication process by dc magnetron sputtering technique has also been included in the current chapter.

The following discussed results have been published in journals in reference [75,211].

3.1 Fabrication of CoTbNi ternary alloy film on Glass and Si substrate.

The RE-TM CoTbNi ternary alloy films have been fabricated on both glass and Si (<100> and <400>) substrates using DC magnetron sputtering. The various targets used in this thesis works are Ni (99.99%), $Co_{85}Tb_{15}$ (99.99%), and Ta (99.99%). The targets used for the fabrication of films were 2 inches in diameter and 4 mm in thickness. The plane glass of thickness 2 mm has been used as a glass substrate. For the Si substrate, Si wafer of 2-inch diameter and 1 mm thickness purchased from Sigma Aldrich has been used for the deposition of the films.

The Ni, $Co_{85}Tb_{15,}$ and Ta targets were fitted to the cathode and the magnetron angles were properly adjusted. The four cut pieces of substrate were fitted on the substrate holder with the help of clamp. The vacuum chamber of the magnetron sputtering unit is evacuated using rotary vane pump to a rough vacuum of order 10^{-2} mbar and then the diffusion pump is switched ON. After 45 minutes the high vacuum valve is opened and the chamber is evacuated to about $5x10^{-5}$ mbar. The Ar gas is then introduced inside the vacuum chamber and allowed vacuum pressure to drop to $3x10^{-2}$ mbar. The gas flow is so adjusted that the vacuum pressure remains stable at $\sim 3x10^{-2}$ mbar. At this pressure, the deposited rate of the film is found to be maximum, and films are deposited uniformly. Once this pressure is adjusted, the negative voltage is applied to the cathodes. The target voltages are increased in step of -10 volt from zero until the first plasma is stroked. The target voltage is then increased in small steps until the bright plasma is produced. The targets are allowed to sputter until the target voltage and plasma current becomes stable. Then the shutter is opened and allowed to deposit the sputtered target material on the substrate. During the deposition of film, the substrate holder is rotated with the help of an electric motor equipped to ensure uniform deposition. The Ni target and $Co_{85}Tb_{15}$ targets are co-sputtered at the same time so as to deposit CoTbNi alloy film. The Ta target is then deposited over the CoTbNi film as a protective layer for oxidation as well as scratches. The schematic diagram of the deposition of film is illustrated in Figure 3.1 below.

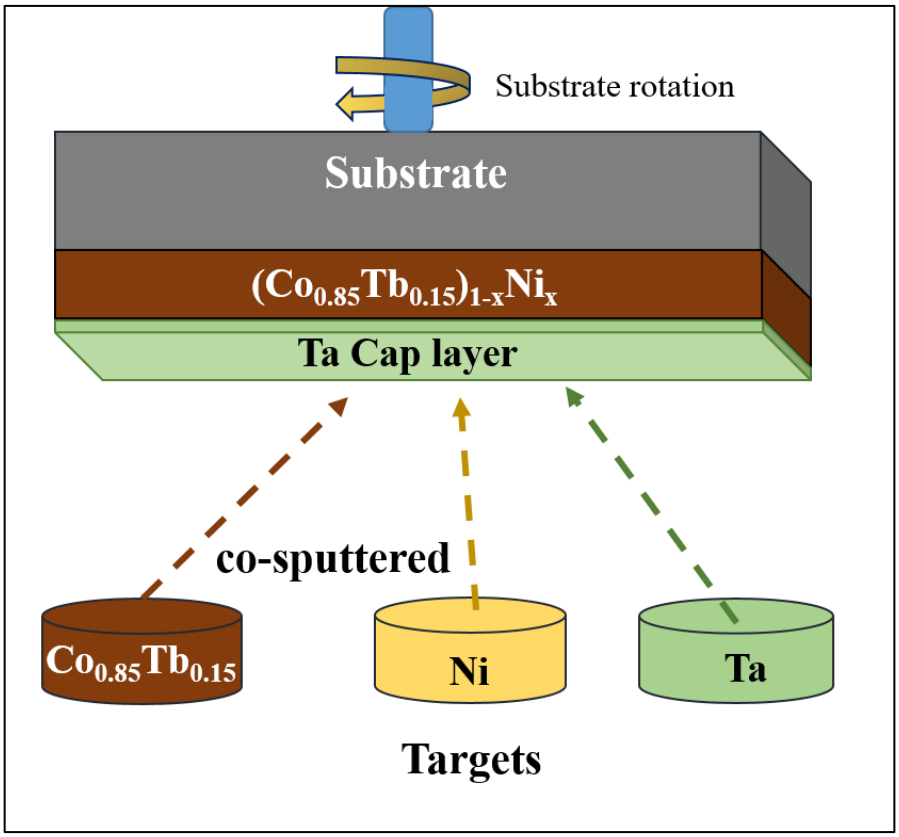

Figure 3.1 Schematic diagram of co-sputtering of CoTbNi ternary alloy using DC magnetron sputtering system.

3.2 Optimization of Deposition Rate of the Films

Optimization of the deposition rate of target material is a vital task before the film is actually deposited. The target material must be sputtered at a particular target voltage (Power) at which the maximum deposition yield is obtained and the thin film is uniformly deposited. Each target used in the deposition of thin film is sputtered at three different target voltages one at which bright plasma is produced and the other two greater by -20V and -40V, maintaining the same vacuum pressure $3x10^{-2}$ mbar. The deposition pressure is adjusted by Ar gas flow and deposited for 30 minutes. The deposition rate per minute is determined for each deposited film and also the uniformity of the thin film is checked using Profilm 3D profilometer. Then the target voltage is selected at which the best deposition rate and uniform films are obtained. To determine the deposition rate and hence the overall thickness of the film, the film is deposited on a partially masked substrate for 30 minutes. The

mask is removed after deposition and the step height formed is measured by step height measurement mode using Profilm 3D profilometer. The same process is repeated three times and the average deposition rate per minute is determined for each film at specified sputtering power of targets. One typical step height deposited and step height measurement of sample-7 is depicted in Figure 3.2. The average deposition rate per minute of the films against each sputtering power is presented in Table 3.1. The deposition rate of the film increases with Ni target power as expected as the higher sputtering power would eject more atoms from the surface of the target material. The actual thin films were then deposited for the desired duration to maintain approximately the same overall thickness for all the prepared thin films. The actual deposition time to maintain overall thickness of 120 nm of all the samples are listed in the Table 3.1. After the deposition of actual thin films, the thickness of the thin films is cross-checked and confirmed by the step height measurement method as mentioned earlier. The scan step height of the actual film is presented in Figure 3.3. The thickness of the film is found to be 120 nm (approx.).

Table 3.1 Deposition rate of each sputtered thin films and deposition time of actual film deposition.

Sample	Sputtering power (watt)		Deposition rate	Deposition time	Thickness (nm)
$(Co_{0.85}Tb_{0.15})_{1-x}Ni_x$	$Co_{85}Tb_{15}$	Ni	(nm/min)	(min/second)	(approx.)
Sample-1	261	293	18.80	6 min 28 sec	120
Sample-2	261	315	19.21	6 min 15 sec	120
Sample-3	261	338	19.60	6 min 7 sec	120
Sample-4	261	383	20.33	5 min 50 sec	120
Sample-5	261	405	21.00	5 min 40 sec	120
Sample-6	261	428	21.67	5 min 30 sec	120
Sample-7	261	450	22.33	5 min 20 sec	120

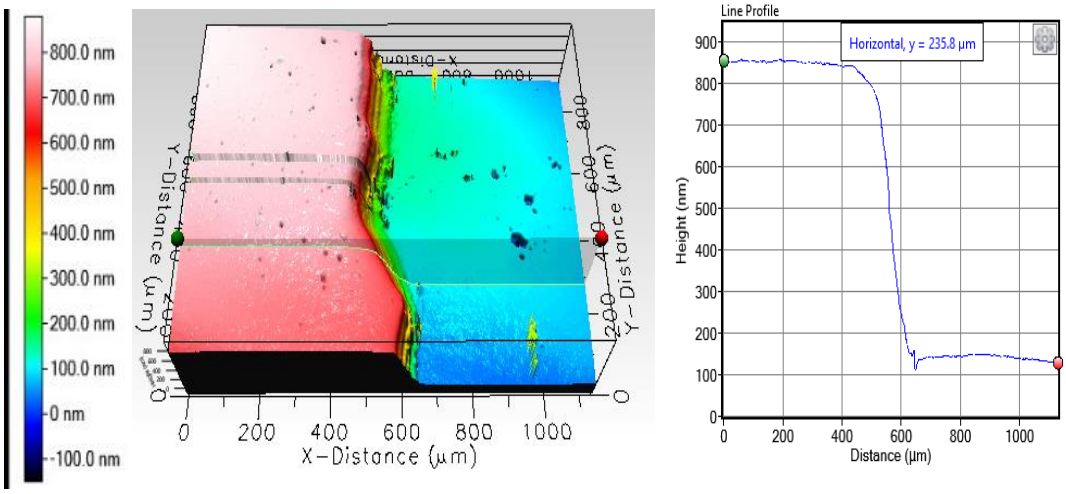

Figure 3.2 3D coloured image of Step height with colour contrast z-scale and line profile of step height of sample-7.

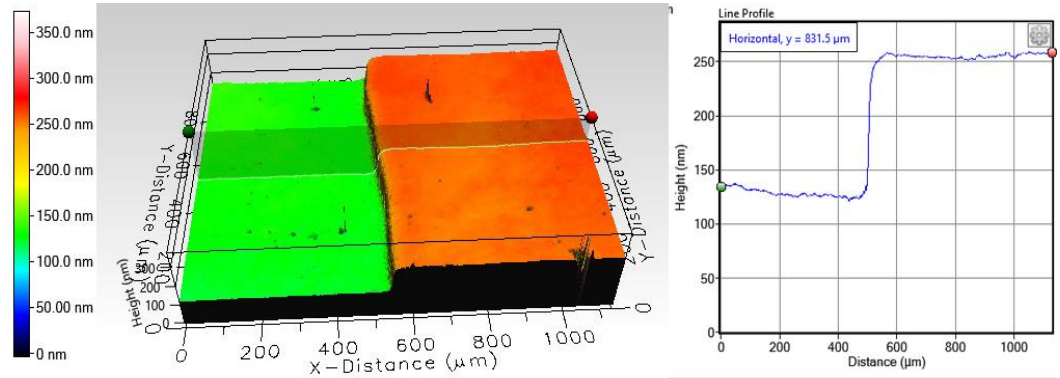

Figure 3.3 3D image of step height (middle) of actual film deposited along with line profile (right) and colour contrast z-scale (left) of sample-7.

3.3 Composition Analysis by EDX

For compositional analysis by EDX, the samples were deposited onto the glass substrates. The deposited samples were cut into small pieces (4 mm x 4 mm approx.). The cut pieces of samples are then attached to the sample holder with the help of carbon tap and then gold coated to facilitate a conductive path for electrons. After the samples are gold coated, the samples are loaded into the vacuum chamber of SEM equipped with EDX. The vacuum chamber is evacuated with the help of Turbo molecular Pump (TMP) to a vacuum pressure of order 10^{-7} mbar. The representative EDX spectra of one of the deposited sample is depicted in Figure 3.4.

The peak of Si and O comes from the substrate used to deposit the film, and the other peaks like Au, C, and Mg arise due to sample preparation for EDX measurement. The spectra do not show any other peaks of foreign elements which signifies that the samples are free from foreign material. To determine the relative composition of the samples the EDX spectra are recorded by removing the unwanted elements (Au, Si, C, O etc.) that are not present in the sample and expressed in atomic percentage. A number of spectra have been recorded at various locations of the samples. The composition of the samples is determined by averaging the relative atomic percentage. The representative EDX spectra of one of the samples are depicted in Figure 3.5, and the determination of composition of the sample is illustrated in Table 3.2. In the same way, the compositions of other samples are also determined. The obtained compositions of all prepared thin films are presented in Table 3.3.

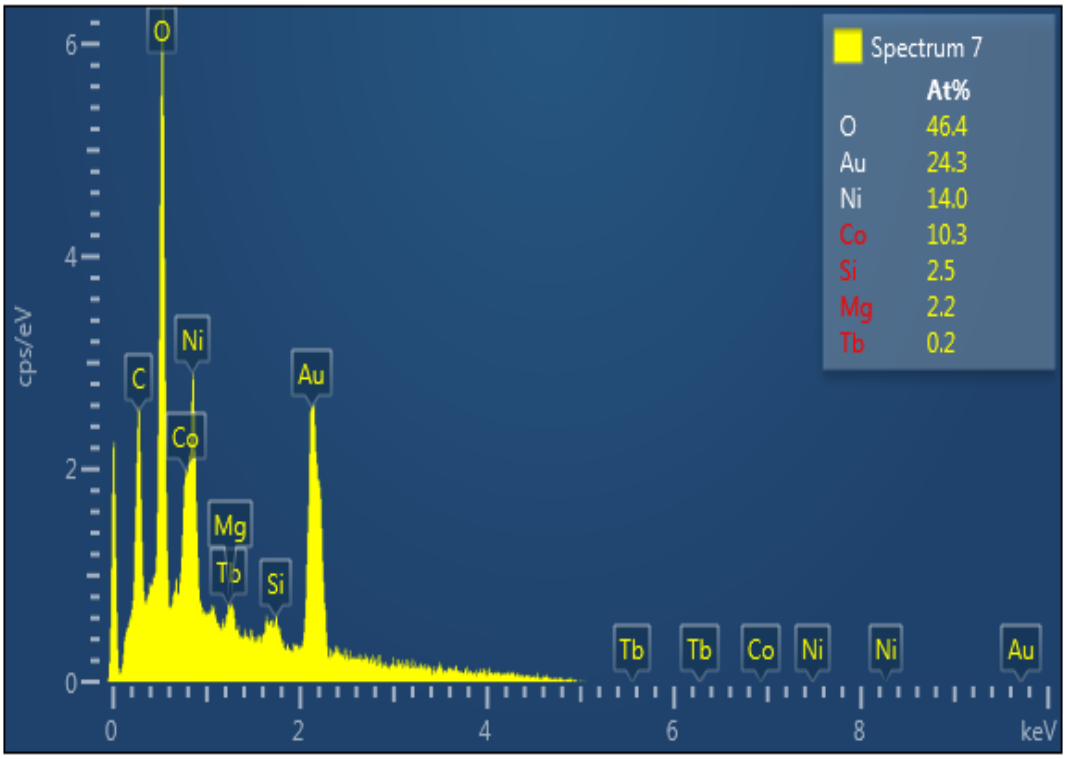

Figure 3.4 EDX spectra of CoTbNi Ternary alloy film without removing the unwanted elements that are not present in the sample.

Table 3.2 Determination of compositions of the CoTbNi alloy thin films using EDX spectra.

Sample	Target voltage (volt)	Spectrum-1	Spectrum-2	Spectrum-3	Spectrum-4	(1+2+3+4)/4	CoTbNi	Composition $(Co_{0.85}Tb_{0.15})_{1-x}Ni_x$
$Co_{0.85}Tb_{0.1}$	261	37.5	39.2	36.6	37.1	37.6	$Co_{0.38}Tb_{0.08}Ni_{0.54}$	$(Co_{0.85}Tb_{0.15})_{0.46}Ni_{0.54}$
		8.3	7.3	8.6	8.0	8.1		
Ni	400	54.2	53.5	54.8	54.8	54.3		

Table 3.3 Compositions of CoTbNi ternary alloy thin films with Ni deposited at different sputtering powers.

Sample	Sputtering power (watt)		Composition of films
$(Co_{0.85}Tb_{0.15})_{1-x}Ni_x$	$Co_{0.85}Tb_{0.15}$	Ni	
Sample-1	261	293	$(Co_{0.85}Tb_{0.15})_{0.74}Ni_{0.26}$
Sample-2	261	315	$(Co_{0.85}Tb_{0.15})_{0.55}Ni_{0.45}$
Sample-3	261	338	$(Co_{0.85}Tb_{0.15})_{0.46}Ni_{0.54}$
Sample-4	261	383	$(Co_{0.85}Tb_{0.15})_{0.40}Ni_{0.60}$
Sample-5	261	405	$(Co_{0.85}Tb_{0.15})_{0.37}Ni_{0.63}$
Sample-6	261	428	$(Co_{0.85}Tb_{0.15})_{0.28}Ni_{0.72}$
Sample-7	261	450	$(Co_{0.85}Tb_{0.15})_{0.19}Ni_{0.81}$

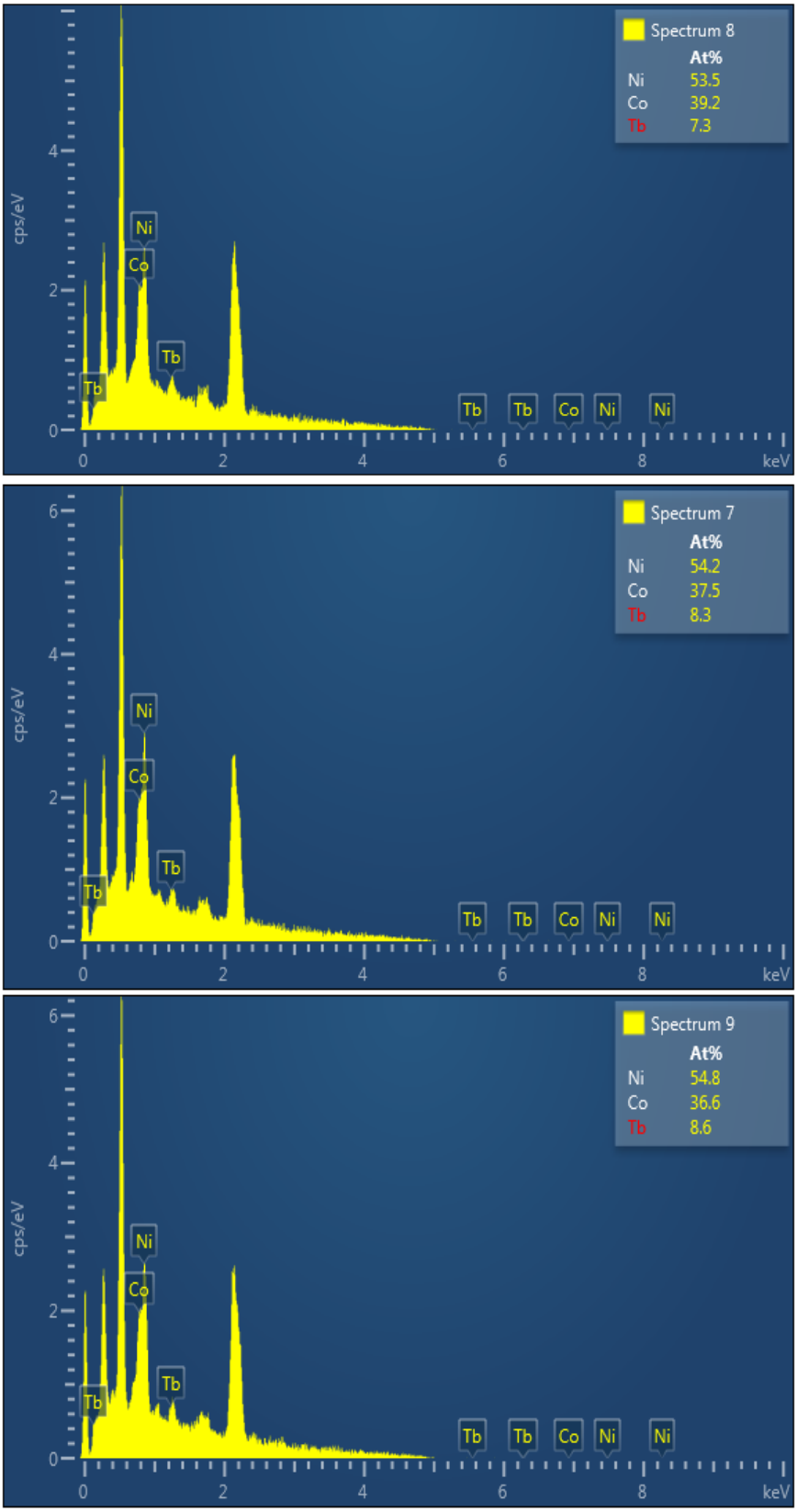

Figure 3.5 EDS spectra of a sample recorded at different locations of the sample to determine the relative composition of the sample.

The elemental colour mapping of the samples have also been recorded. The elemental colour mapping of EDX spectra gives the distribution of elements present in the sample and shows the uniformity and homogeneity of the sample. One representative elemental colour map image has been illustrated in Figure 3.6. The Co, Ni, and Tb atoms are seen to be uniformly distributed and no concentration of particular elements at some particular location within the scan area of the sample is seen.

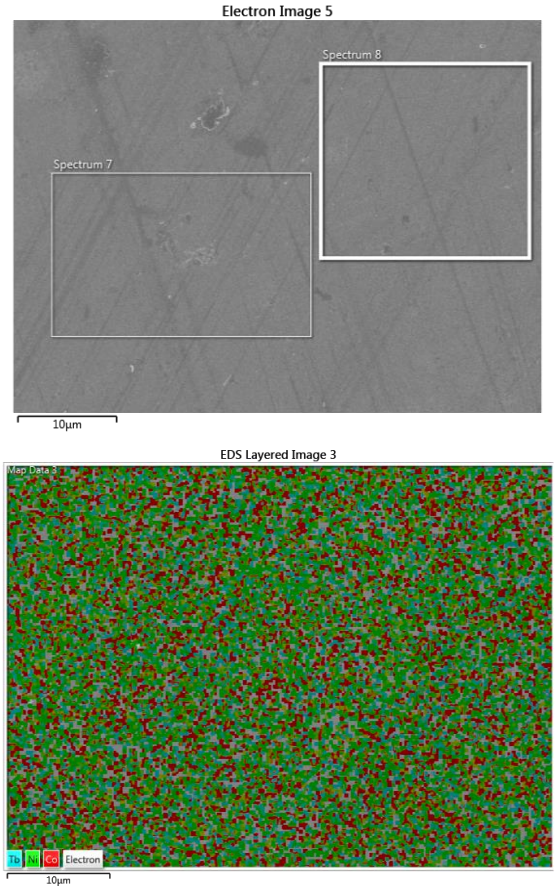

Figure 3.6 Raw SEM image (top) and EDS Elemental colour mapping spectra (bottom) of $(Co_{0.85}Tb_{0.15})_{0.46}Ni_{0.54}$ alloy thin film.

3.4 Surface Topography and Surface Roughness Measurement by 3D Optical Profilometer

The surface topography and the film surface roughness have been measured by using Profilm 3D optical profilometer. The measurement was carried out by using the phase shifting interferometry (PSI) mode of scan. The film surface is captured

by an integrated 4x Nikon DI objective lens. The $200\,\mu m \times 200\,\mu m$ area of the sample is selected and the S_a and R_a of the sample surface are measured in ISO 25178 Height and ISO 4287 Amplitude standard respectively. S_a is the arithmetic mean/average of the absolute distances of the surface points from the mean plane [212]. The equation by which S_a [212] is measured by

$$S_a = \frac{1}{MN}\sum_{j=1}^{N}\sum_{N=1}^{M}|z|(x_i, y_j) \tag{3.1}$$

Where, M and N are the numbers of columns and rows respectively in the film surface within the scanned area of the sample. The R_a on the other hand is the arithmetic mean of absolute ordinate values Z(x) within the sampling length [185]. The equation by which R_a [185] is measured is

$$R_a = \frac{1}{l}\int_{0}^{l}|Z(x)|dx \tag{3.2}$$

Where l is the sampling length.

3.4.1 Surface Topography and Surface Roughness of As-deposited CoTbNi Films

The coloured 3D image of surface (middle panel) topography with colour contrast z-scale (left panel) and line profile (right panel) of the as-deposited thin films are depicted in Figure 3.7 to Figure 3.13 and the obtained surface roughness parameters are presented in Table 3.4. The value of R_a may slightly differ from point to point depending on the position of the line at which the measurement is done. So for the best result, the line profile is measured in the middle of the scan area of the sample. The colour contrast of the film gives the qualitative indication of the height of film surface and hence the roughness of the film surface. The S_a value of the first three deposited thin films x=0.26, 0.45, and 0.60 are 1.083, 1.632, and 1.376 nm respectively and respective R_a values are 0.463, 0.735, and 0.487 nm. The other four thin films x=0.54, 0.63, 0.72, and 0.81 possess S_a =1.579, 1.714, 3.044, 0.648 nm and R_a= 0.528, 0.581, 0.364 and 0.570 nm respectively. The film surface

roughness S_a varies in the range of 0.648−3.044 nm and R_a in the range of 0.364−0.735 nm which is sufficiently small as compared to the thickness of films. The variations of surface roughness parameters S_a and R_a of the as-deposited films are plotted as a function of Ni-content of the films in Figure 3.14. The value of S_a is higher than the R_a value for all the samples. An overall increase in S_a is observed with increase in Ni content up to x=0.72. for x=0.81 film, the S_a steeply decreases. On the other hand, the R_a shows a gradual decrease with the increase in Ni content of the films. The x=0.81 film possesses nearly the same S_a and R_a.

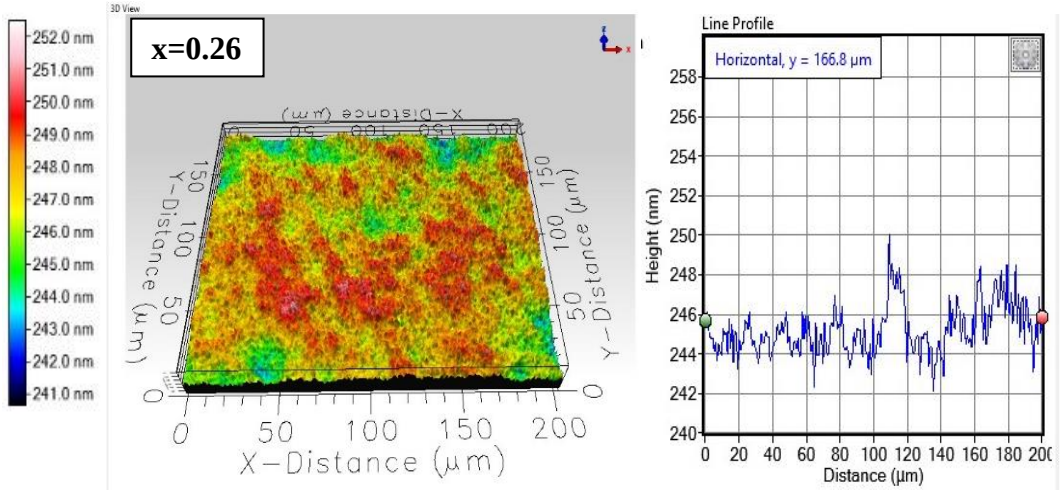

Figure 3.7 3D coloured image of surface topography with colour contrast z-scale and line profile of as-deposited x=0.26 thin film.

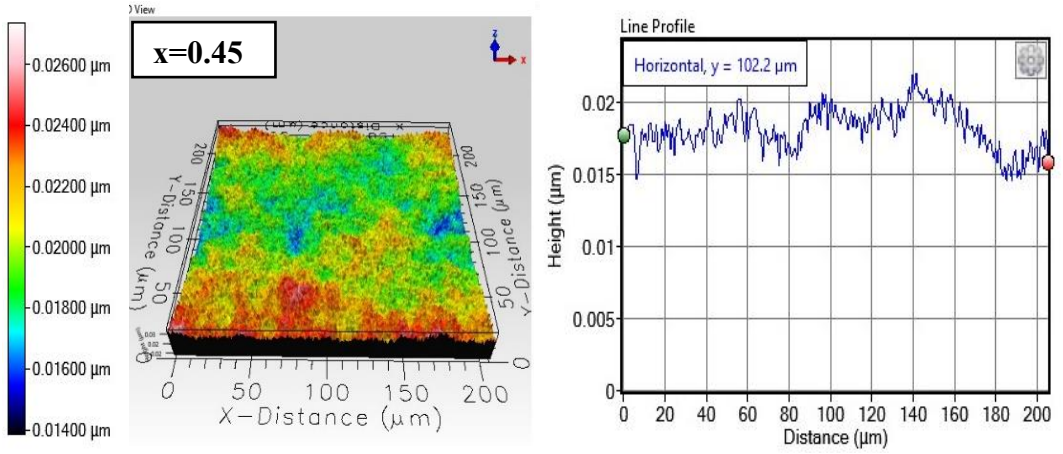

Figure 3.8 3D coloured image of surface topography with colour contrast z-scale and line profile of as-deposited x=0.45 thin film.

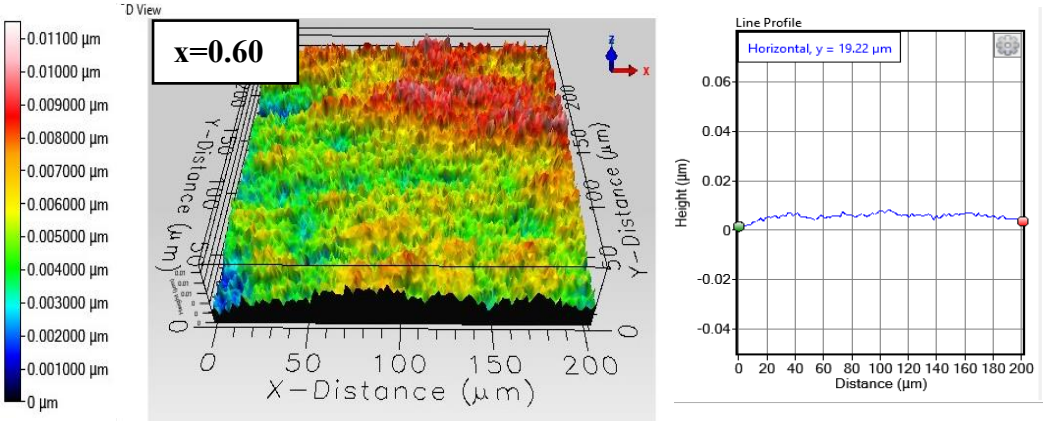

Figure 3.9 3D coloured image of surface topography with colour contrast z-scale and line profile of as-deposited x=0.60 thin film.

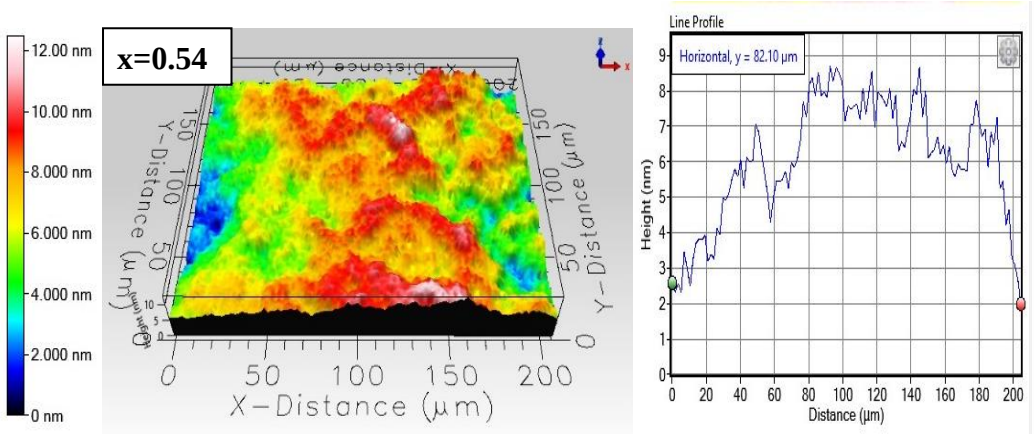

Figure 3.10. 3D coloured image of surface topography with colour contrast z-scale and line profile of as-deposited x=0.54 thin film.

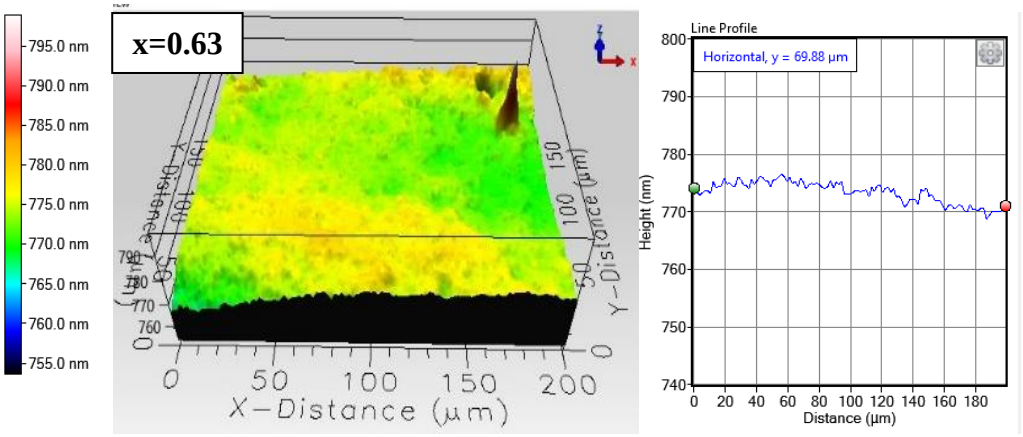

Figure 3.11. 3D coloured image of surface topography with colour contrast z-scale and line profile of as-deposited x=0.63 thin film.

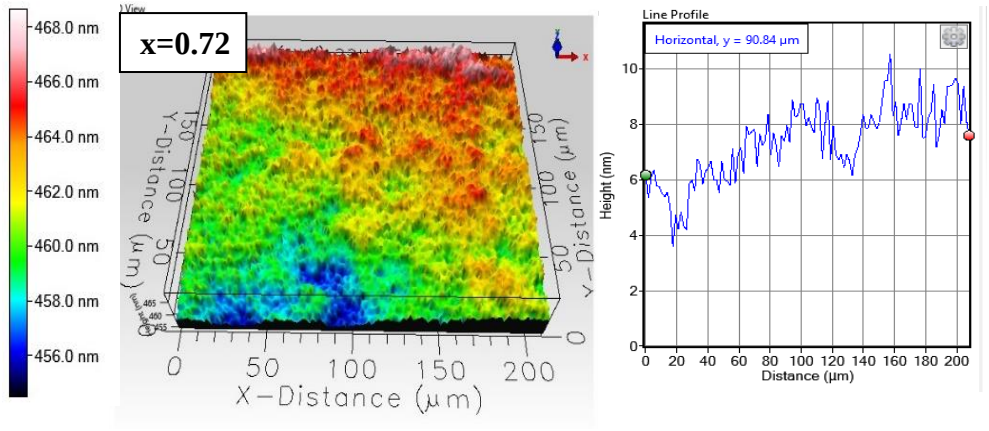

Figure 3.12 3D coloured image of surface topography with colour contrast z-scale and line profile of as-deposited x=0.72 thin film.

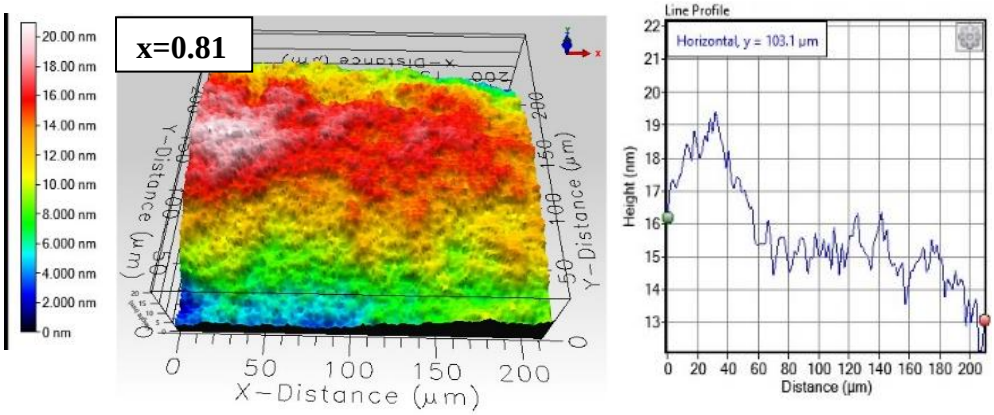

Figure 3.13 3D coloured image of surface topography with colour contrast z-scale and line profile of as-deposited x=0.81 thin film.

Table 3.4 Surface roughness parameters S_a and R_a of as-deposited CoTbNi thin films obtained by 3D optical profilometer.

Sample $(Co_{0.85}Tb_{0.15})_{1-x}Ni_x$	Surface roughness	
	As-deposited	
	S_a (nm)	R_a (nm)
x=0.26	1.083	0.846
x=0.45	1.632	0.735
x=0.60	1.376	0.487
x=0.54	1.579	0.528
x=0.63	1.714	0.581
x=0.72	3.044	0.364
x=0.81	0.648	0.570

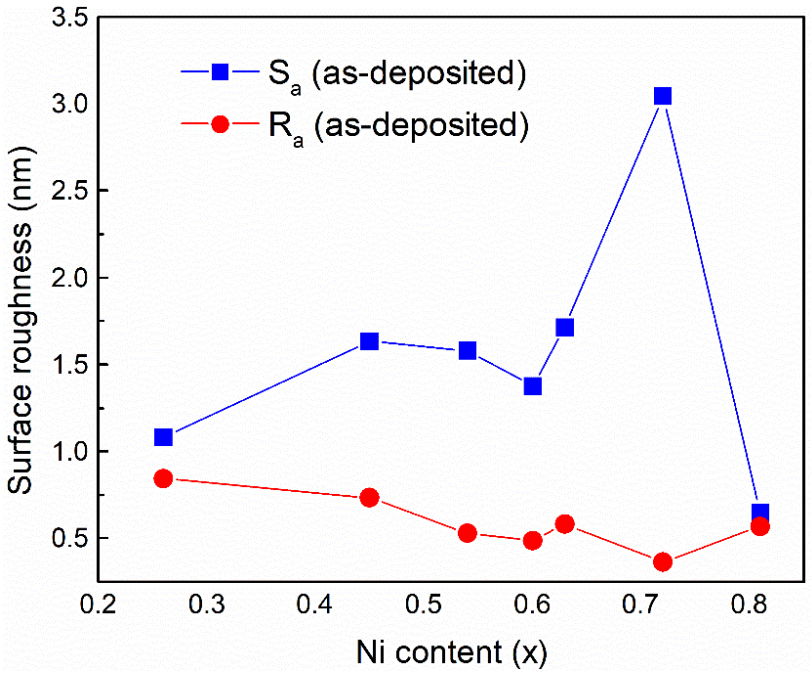

Figure 3.14 Plot of variation of S_a and R_a as a function of Ni content of the as-deposited thin films.

3.4.2 Surface Topography and Surface Roughness of In-situ Post Annealed CoTbNi Films

The 3D coloured images of film surface topography with colour contrast z-scale of all in-situ post-annealed samples are presented in Figure 3.15. The obtained values of S_a and R_a of the annealed films are presented in Table 3.1. The annealing of samples of composition x=0.26, 0.45, and 0.60 was not carried out due to isotropic magnetic behaviour which will be discussed in section 3.2. The obtained values of S_a of annealed x=0.54, 0.63, 0.72, and 0.81 films are 0.952, 1.077, 1.195, and 1.358 nm respectively and the respective average line roughness R_a are 0.401, 0.438, 0.418 and 0.531 nm. To analyze the compositional variation of film surface roughness the obtained values of S_a and R_a are plotted as a function of Ni content of the films in Figure 3.16 Plot of variation of surface roughness parameters Sa and Ra of in-situ post annealed films as a function of Ni content.Figure 3.16. It is observed that both S_a and R_a of annealed films increase linearly with an increase in Ni content of the films. The S_a values are found to be greater than the values of R_a as expected. The increase in S_a and R_a with Ni content is attributed to the sputtering of Ni at higher power.

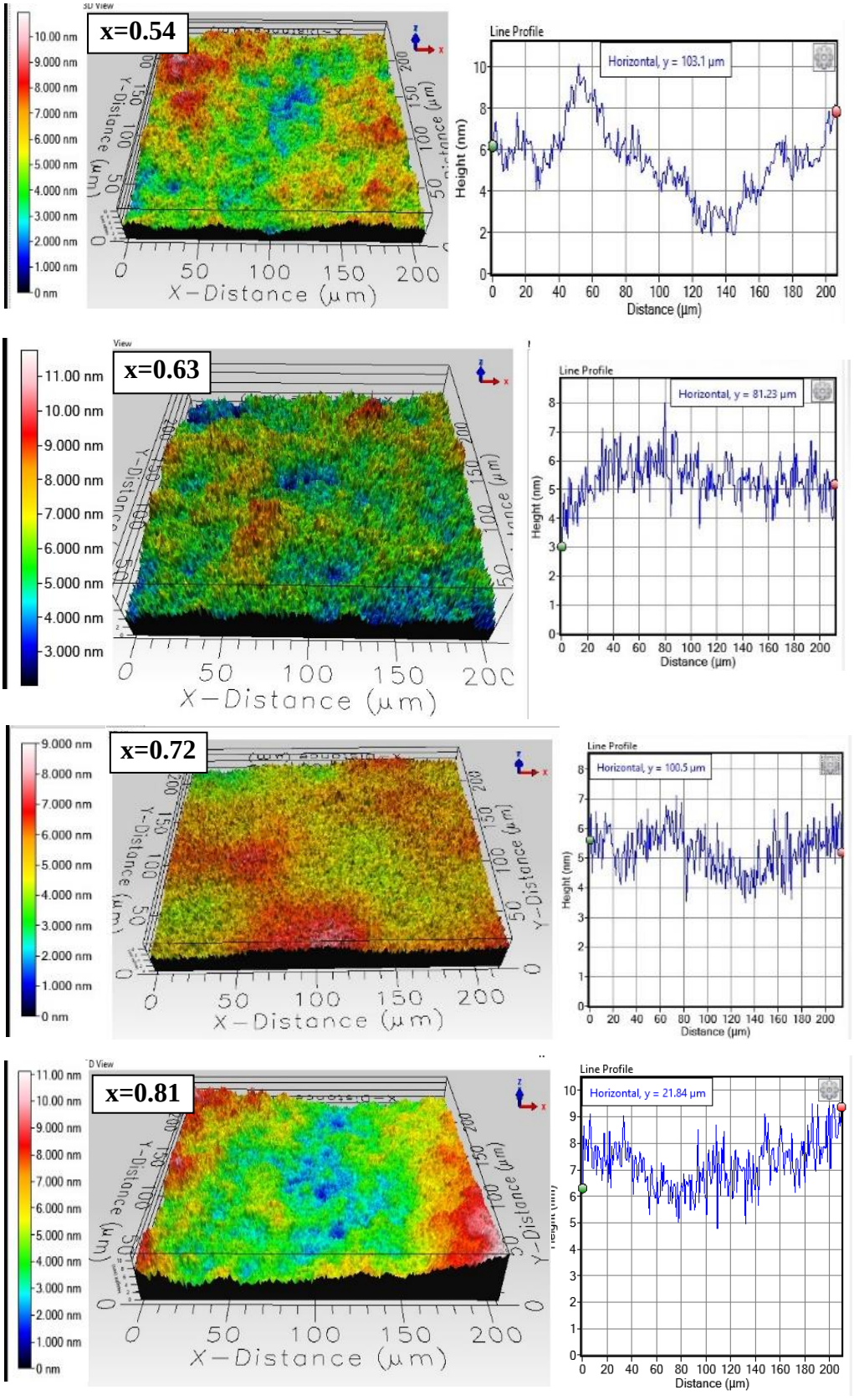

Figure 3.15 3D coloured image of surface topography with colour contrast z-scale of all in-situ post annealed thin film.

Table 3.5 Surface roughness of in-situ post annealed CoTbNi films obtained by 3D optical profilometer.

Sample $(Co_{0.85}Tb_{0.15})_{1-x}Ni_x$	In-situ post annealed	
	Surface Roughness	
	S_a (nm)	R_a (nm)
x=0.54	0.952	0.401
x=0.63	1.077	0.438
x=0.72	1.195	0.418
x=0.81	1.358	0.531

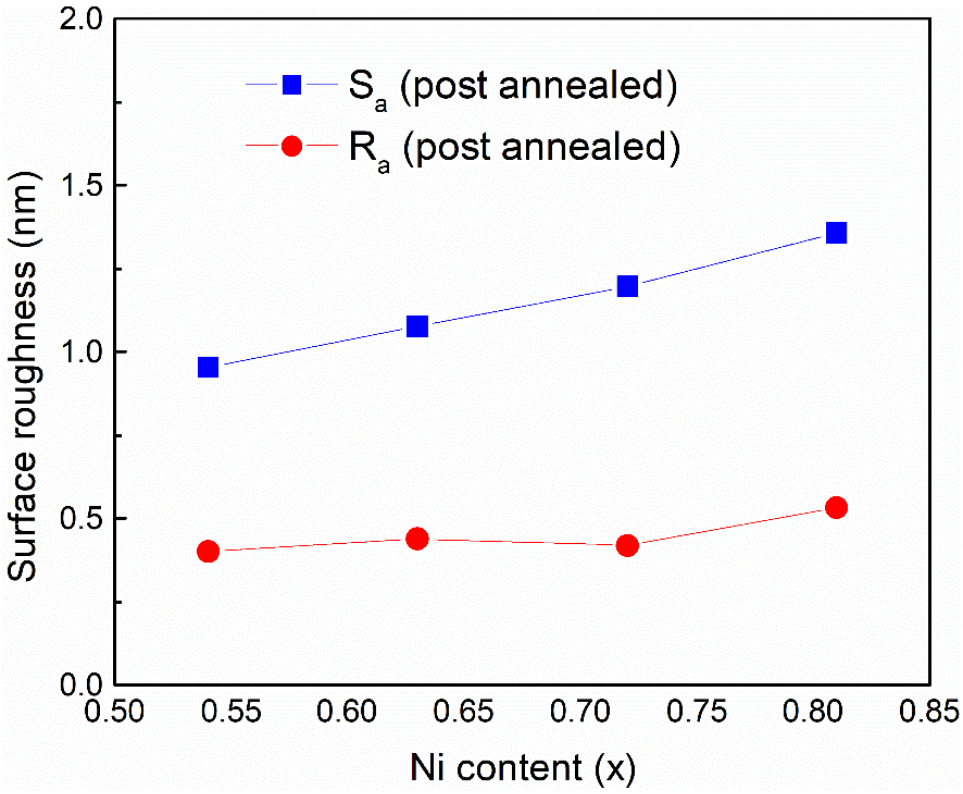

Figure 3.16 Plot of variation of surface roughness parameters S_a and R_a of in-situ post annealed films as a function of Ni content.

3.4.3 Influence of Post annealing on Film Surface Roughness

To analyze the influence of post-annealing of the films on surface roughness, the S_a and R_a of both as-deposited and annealed thin films are plotted as a function of Ni content and presented in Figure 3.17. Both as-deposited and annealed thin films show increasing S_a with the increase in Ni content. However, S_a of as-deposited x=0.81 sample decreases steeply. Moreover, annealed films possess a smaller S_a value than as-deposited films. The R_a of both as-deposited and annealed films show an overall increasing trend with an increase in Ni content except for x=0.72. The R_a of annealed films is also found to be smaller than as-deposited films. The post-annealing of thin films causes loosely bound surface atoms to migrate thereby reducing the grain size as described in [213–215]. This results in smaller film surface roughness of annealed thin films.

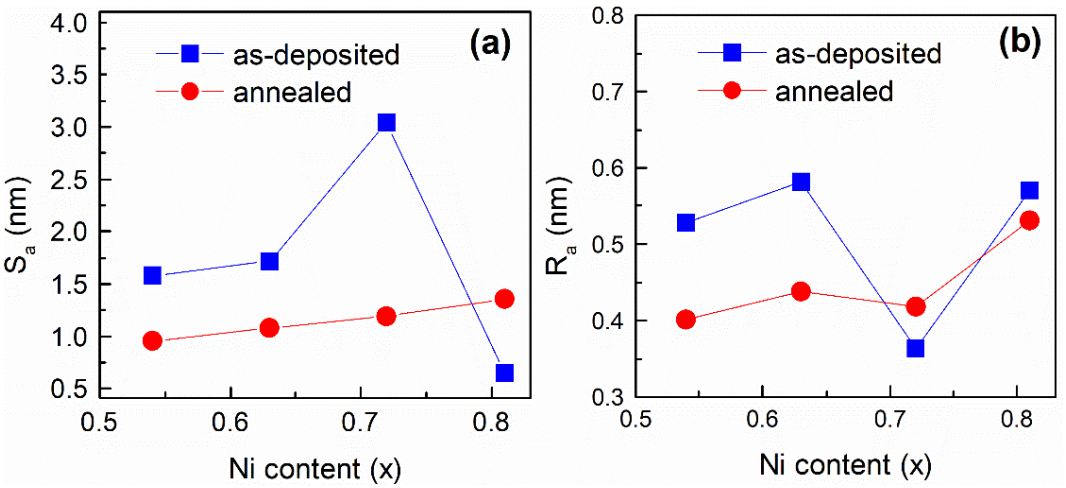

Figure 3.17 Comparative plot of (a) S_a and (b) R_a as a function of as-deposited and in-situ post annealed CoTbNi thin films.

3.5 Crystal Structural Analysis by XRD

3.5.1 Crystal Structure of As-deposited CoTbNi Thin Films

To record the X-ray diffraction profile, the samples were deposited on Si-substrate and are cut into $(1\text{cm} \times 1\text{cm})$ pieces. The X-ray diffraction profiles of the samples are recorded at $2\theta = 5° - 85°$ with scan step of $0.04°$ at room temperature. The obtained XRD patterns of as-deposited films are presented in Figure 3.18. Broad

maxima are observed in the XRD profiles below $2\theta = 30°$ angles. Such broad maxima are typically observed in amorphous materials such as $Co_{0.85}Tb_{0.15}$. The intense peak observed at $2\theta \approx 69°$ is reflection of Si<400> substrate. Additional peaks are observed at $2\theta \approx 33°, \text{and } 61°$ are usually observed in the XRD profile of Si-wafer [216]. No other peaks are observed in the diffraction pattern for all as-deposited samples. This shows that the addition of Ni to $Co_{0.85}Tb_{0.15}$ alloy does not change the crystal structure. Thus the CoTbNi ternary alloy films are amorphous in nature.

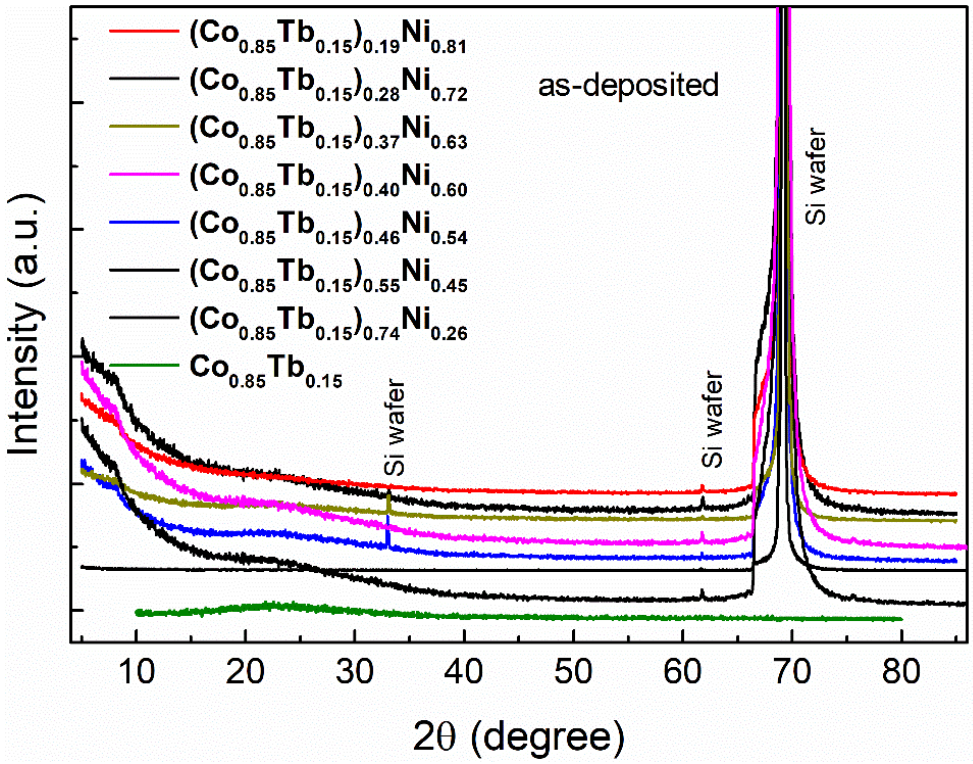

Figure 3.18 X-ray diffraction profile of as-deposited CoTbNi ternary alloy thin films.

3.5.2 Crystal Structure of In-situ Post-annealed CoTbNi Thin Films

The XRD profile of in-situ post-annealed samples CoTbNi thin films are also recorded at $2\theta = 5° - 85°$ with the same scan step of $0.04°$ at room temperature. The obtained XRD patterns of post-annealed thin films are presented in Figure 3.19. Similar broad maxima are observed in XRD profile of in-situ post-annealed samples as that of as-deposited samples which is the signature of amorphous nature. Other

low-intensity peaks are observed at $2\theta \approx 33°, 61°$ similar to those observed in as-deposited samples and are also reflections from Si-substrate. The intense peak at $2\theta \approx 69°$ is reflection from S<400> substrate. This observation also shows that the post-annealed samples are amorphous in nature. The structure of the CoTbNi ternary alloy films is confirmed to be amorphous and does not change upon annealing. Thus post annealing of CoTbNi ternary alloy films at temperature of 673K has no influence on the crystal structure of these films. The observation of amorphous nature of CoTbNi alloy films agrees with other works reported in [216–218].

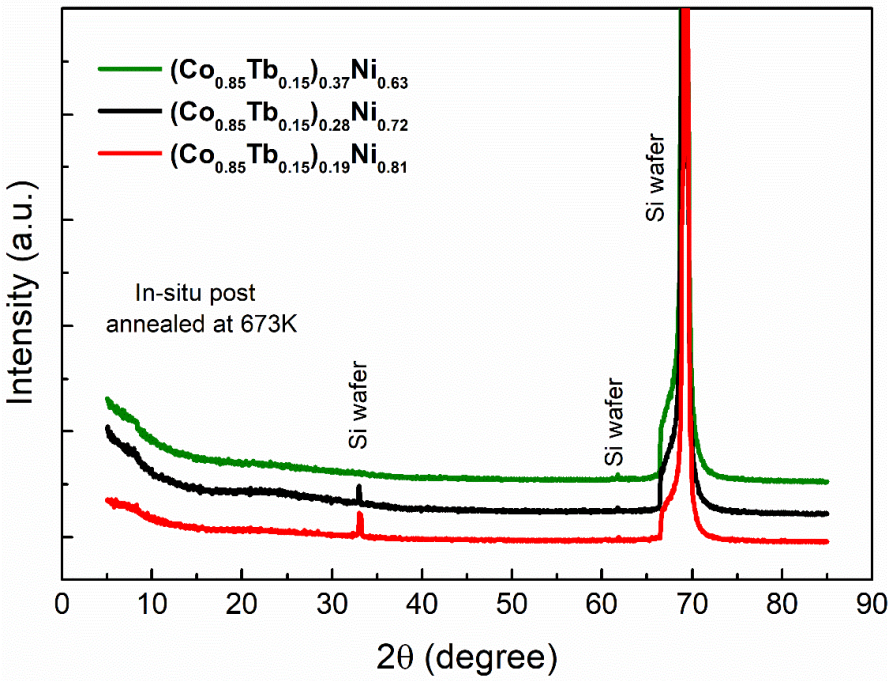

Figure 3.19 Room temperature XRD profile of In-situ post annealed CoTbNi ternary alloy films.

3.6 Magnetic Properties of the CoTbNi Ternary Alloy Film

3.6.1 M-H Measurement Results of As-deposited CoTbNi Films

The hysteresis loop (M-H curves) of the CoTbNi ternary alloy films are measured at room temperature (RT) using VSM. The M-H measurements were carried out in two directions, one by applying external magnetic field parallel to the plane of thin film, and the obtained hysteresis curve is called as in-plane M-H loop. The other

measurement is done by applying magnetic field perpendicular to the plane of film and obtained hysteresis loop is called an out-of-Plane M-H loop. Both the measurements were done at room temperature in the applied field range of 0−1.5 kOe. The RT M-H loops of as-deposited x=0.26, 0.45, x=0.54 and 0.60 thin films have been presented Figure 3.20. The magnetization of the film is expressed in the unit of emu per cubic centimeter (emu/cc) as a function of applied field in the unit of Oersted (Oe). Referring to Figure 3.20, the clear M-H hysteresis loops of these three thin films indicate that they all exhibit RT ferromagnetism. The obtained RT magnetic parameters are presented in Table 3.6. The saturation magnetizations of 194, 87, 1170, and 221 emu/cc are observed for x=0.26, 0.45, and 0.60 films with coercivities of 49, 92, 140, and 59 Oe respectively. These films also possess small remanent magnetization of 15, 7, 134, and 11 emu/cc for x=0.26, 0.45, 0.54 and 0.60 respectively and hence exhibit M-H hysteresis loop of small squareness (M_r/M_S). These observed magnetic parameters indicate that they are soft ferromagnetic materials. The in-plane and out-of-plane M-H curves of these films are found to saturate at the same applied magnetic field. This indicates that all these three thin films exhibit magnetic isotropy.

Table 3.6 Coercivity (H_C), saturation magnetization (M_S), remanent magnetization (M_r) and squareness (M_r/M_S) of as-deposited $(Co_{0.85}Tb_{0.15})_{1-x}Ni_x$ thin films obtained from RT M-H measurement.

Sample $(Co_{0.85}Tb_{0.15})_{1-x}Ni_x$	H_C (Oe)	M_S (emu/cc)	M_r (emu/cc)	M_r/M_S
x=0.26	49	194	15	0.08
x=0.45	92	87	7	0.08
x=0.54	140	1170	134	0.11
x=0.60	59	221	11	0.05

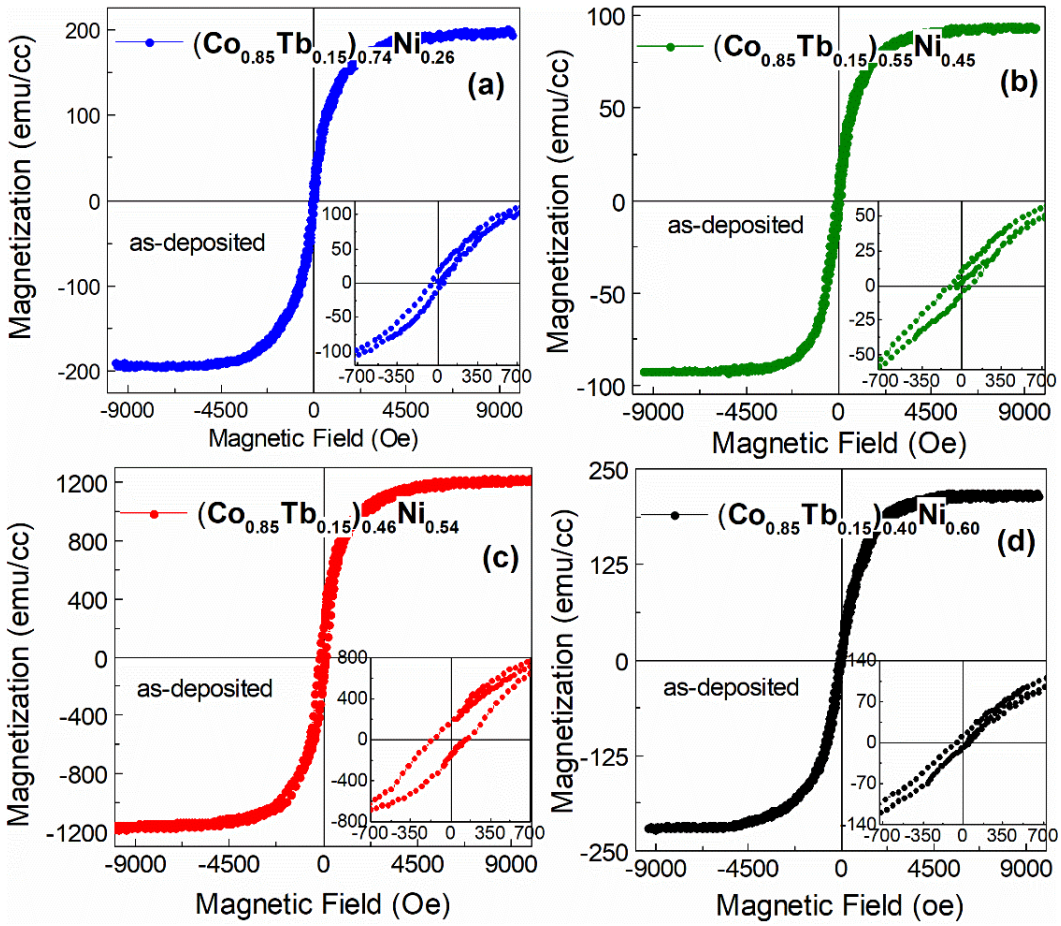

Figure 3.20 Room temperature M-H hysteresis loop of $(Co_{0.85}Tb_{0.15})_{1-x}Ni_x$ films with (a) x=0.26, (b) x=0.45, (c) x=0.54 and (d) x=0.60.

The in-plane and out-of-Plane M-H loop of $(Co_{0.85}Tb_{0.15})_{0.37}Ni_{0.63}$ thin film measured at room temperature have been presented in Figure 3.21. The $(Co_{0.85}Tb_{0.15})_{0.37}Ni_{0.63}$ also exhibits room temperature ferromagnetism. The magnetization is saturated at 890 emu/cc which is lower than the $(Co_{0.85}Tb_{0.15})_{0.46}Ni_{0.54}$ sample. The coercivity and the remanent magnetization of the in-plane M-H loop are found to be 212 Oe and 127 emu/cc and that of out-of-plane M-H loop are 141 Oe and 95 emu/cc respectively. The observed coercive field of this film indicates that the sample is soft room temperature ferromagnetic and the unequal H_C indicates that the sample is magnetically harder in in-plane direction. It is also observed that the in-plane and out-of-plane magnetization do not saturate at the same applied magnetic field. The in-plane magnetization is found to saturate at about 10 kOe. Whereas the out-of-plane magnetization saturates at a much lower

applied field at about 6 kOe. It is observed that both H_C and saturation field is higher in in-plane direction than that when magnetic field is applied perpendicular to the plane of film. This is the signature of magnetic anisotropy with an easy axis along perpendicular to the plane of film and the hard axis parallel to the plane of the film. Thus the $(Co_{0.85}Tb_{0.15})_{0.37}Ni_{0.63}$ thin film exhibits perpendicular magnetic anisotropic (PMA). The effective anisotropic constant (K_{eff}) of the film is calculated by finding the area difference enclosed by the out-of-plane and in-plane M-H curves as described in [11,29–32,80].

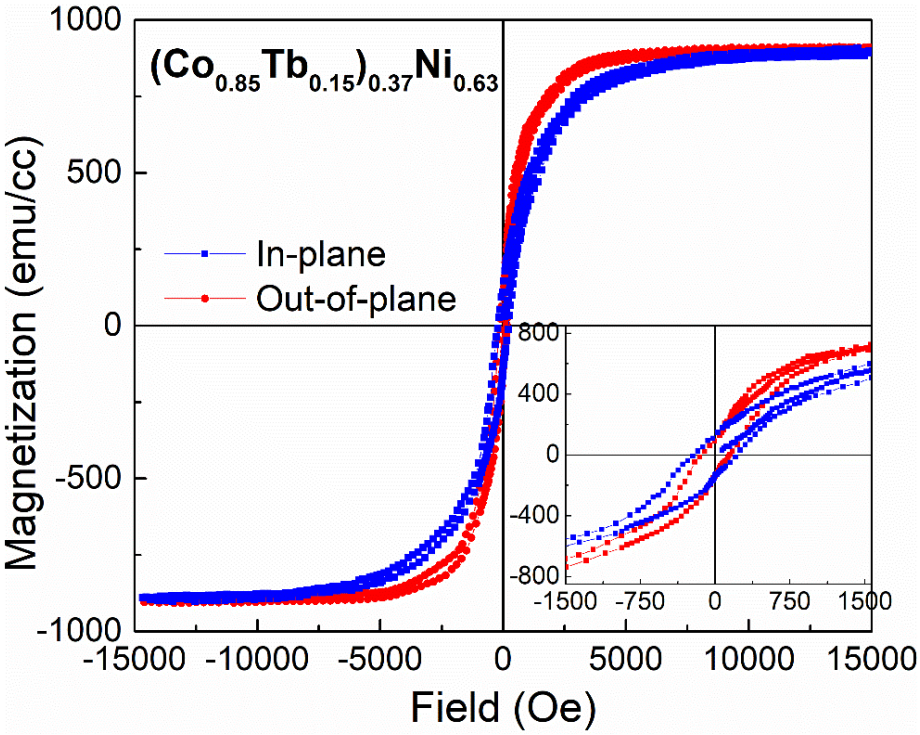

Figure 3.21 In-plane and out-of-plane M-H hysteresis loop of as-deposited $(Co_{0.85}Tb_{0.15})_{0.37}Ni_{0.63}$ thin film measured at room temperature.

To calculate the effective anisotropic constant, only the initial magnetizations of both in-plane and out-of-plane M-H loops are considered. Then the difference in area enclosed by the out-of-plane and in-plane magnetization curves is calculated by integrating the initial magnetization curves and x-axis using Originlab software. This area difference enclosed by the two initial magnetization curves is the indicative value of effective anisotropic constant. The integrated M-H curves are presented in Figure 3.22. The shaded region in grey colour in Figure 3.22 represents

the calculated difference in area enclosed by initial out-of-plane and in-plane M-H curves which is the approximate measure of K_{eff}. The value of K_{eff} for $(Co_{0.85}Tb_{0.15})_{0.37}Ni_{0.63}$ film is found to be 7.75×10^5 erg/cc.

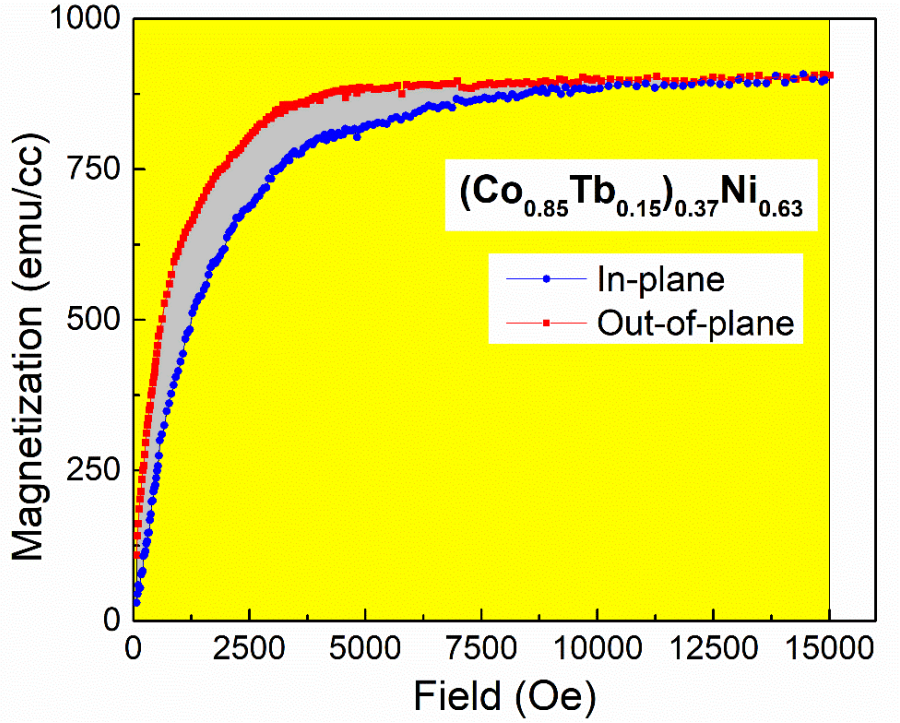

Figure 3.22 Calculation of area difference enclosed by in-plane and out-of-plane initial magnetization curves of $(Co_{0.85}Tb_{0.15})_{0.37}Ni_{0.63}$ alloy thin film.

The room temperature M-H hysteresis loops of x=0.72 film are presented in Figure 3.23. The 72 at. % Ni content sample i.e., $(Co_{0.85}Tb_{0.15})_{0.28}Ni_{0.72}$ sample also exhibit soft ferromagnetism at room temperature. The coercive field of this film in the in-plane M-H loop is found to be 74 Oe, which increases to 145 Oe when measured in out-of-plane direction. The out-of-plane magnetization is found to saturate at 431 emu/cc at a much lower applied field (~ 8000 Oe) as compared to the in-plane Magnetization which is found to saturate at (~ 12000 Oe). This clearly indicates that the thin film with 72 at. % Ni-content also exhibits perpendicular magnetic anisotropy. The effective anisotropic constant of this film is also calculated from M-H curves using the same process as detailed for the film with Ni 63 at. %. The calculation of K_{eff} by integrating initial M-H curves is presented in Figure 3.24. The calculation of K_{eff} from M-H hysteresis loop gives 5.90×10^5 erg/cc. The remanent

magnetization of this film is also greater (44 emu/cc) in out-of-plane direction than the in-plane magnetization (15 emu/cc). This clearly shows that the out-of-plane M-H loop exhibit better squareness (0.102) than the in-plane M-H loop (0.034).

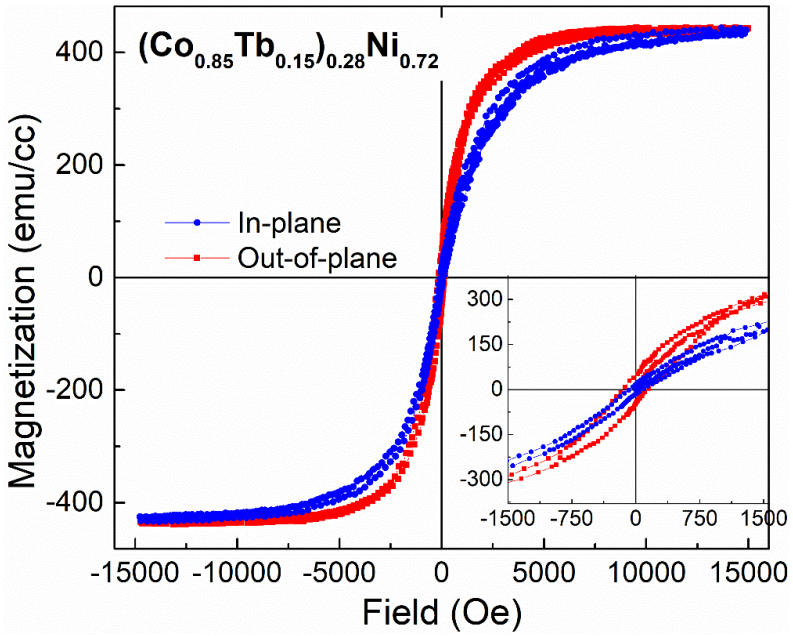

Figure 3.23 In-plane and out-of-plane M-H hysteresis loop of as-deposited $(Co_{0.85}Tb_{0.15})_{0.28}Ni_{0.72}$ alloy film measured at room temperature.

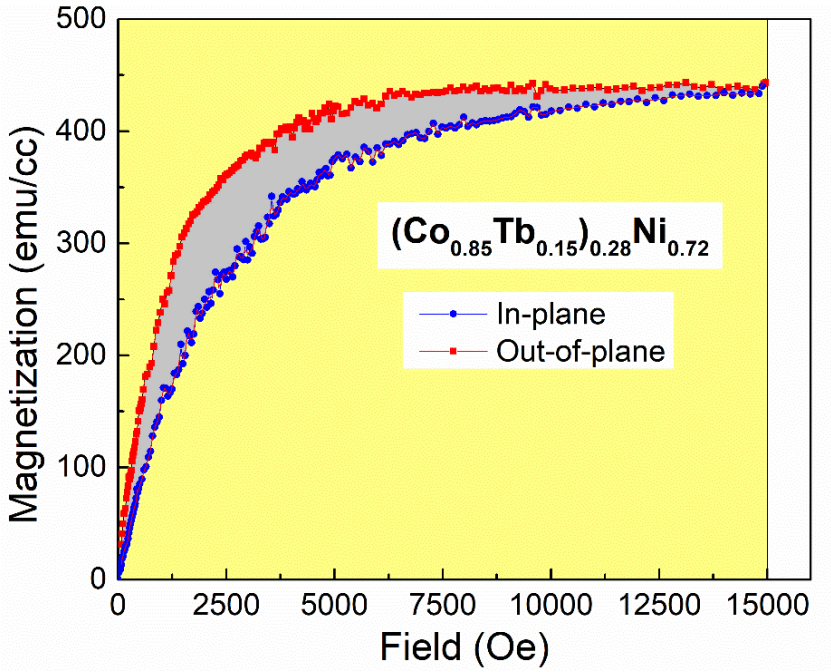

Figure 3.24 Calculation of area difference enclosed by in-plane and out-of-plane initial magnetization curves of $(Co_{0.85}Tb_{0.15})_{0.28}Ni_{0.72}$ alloy thin film.

The $(Co_{0.85}Tb_{0.15})_{0.19}Ni_{0.81}$ film with 81 at. % Ni content also exhibits soft ferromagnetism as indicated by Figure 3.25. The obtained magnetic parameters are presented in Table 3.7. The coercivity and remanent magnetization of this film is found to be 120 Oe and 23 emu/cc in In-plane which increases to 150 Oe and 43 emu/cc respectively in out-of-plane measurement. From Figure 3.25, it is also clearly seen that the magnetization curve saturates at 399 emu/cc at a lower applied field in out-of-plane direction than in-plane direction. This indicates that the film has a magnetic easy axis along the perpendicular direction and hence exhibits PMA. To quantify the PMA, the effective anisotropic constant of this film is also calculated from M-H curves using the same process as detailed for the film with Ni 63 at. %. The calculation of K_{eff} by integrating initial M-H curves is presented in Figure 3.26. The calculation of K_{eff} from M-H hysteresis loop gives 2.45×10^5 erg/cc. The squareness of the in-plane M-H loop of the film is 0.06 and that of out-of-plane M-H loop is 0.1. This shows that the film has better squareness in perpendicular direction.

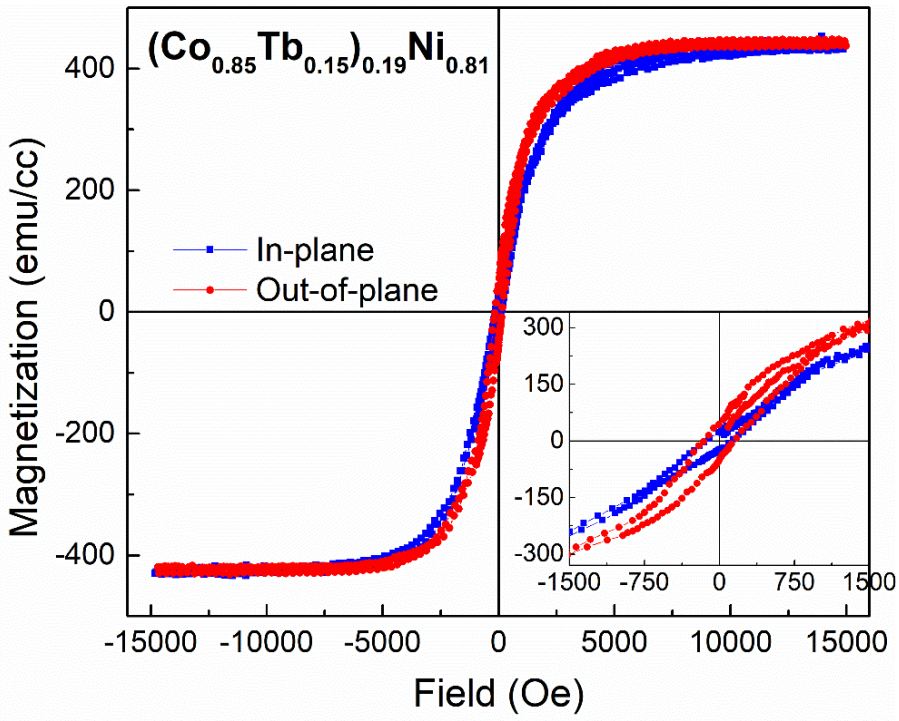

Figure 3.25 In-plane and out-of-plane M-H hysteresis loop of as-deposited $(Co_{0.85}Tb_{0.15})_{0.19}Ni_{0.81}$ alloy thin film measured at room temperature.

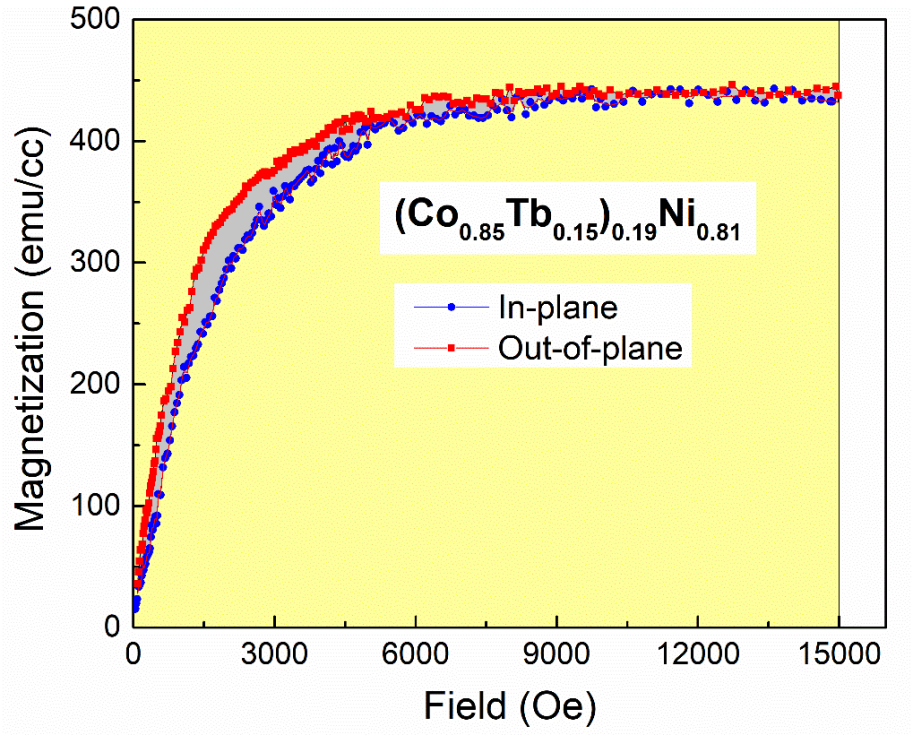

Figure 3.26 Calculation of area difference enclosed by in-plane and out-of-plane initial magnetization curves of $(Co_{0.85}Tb_{0.15})_{0.19}Ni_{0.81}$ alloy thin film.

Table 3.7 Room temperature magnetic parameters of as-deposited $(Co_{0.85}Tb_{0.15})_{1-x}Ni_x$ alloy thin films. The IP and OOP represent in-plane and out-of-plane respectively.

Magnetic Parameters	$(Co_{0.85}Tb_{0.15})_{1-x}Ni_x$ samples					
	x=0.63		x=0.72		x=0.81	
	IP	OOP	IP	OOP	IP	OOP
H_C (Oe)	212	141	74	145	120	150
M_r (emu/cc)	127	95	15	44	23	43
M_S (emu/cc)	890		431		399	
M_r/M_S	0.14	0.12	0.03	0.10	0.06	0.11
K_{eff} (erg/cc)	7.75×10^5		5.90×10^5		2.45×10^5	

To analyze the compositional dependence of magnetic properties of as-deposited CoTbNi thin films, the obtained room temperature magnetic parameters are plotted as a function of Ni content in atomic percentage. From Figure 3.27, it is clear that the out-of-plane coercive field of as-deposited films first decreases with an increase in Ni-content of the film up to 63 at. % and then gradually increases with increase in Ni-content systematically. However, the H_C of in-plane M-H loop first increases with an increase in Ni-content of the film for 63 at. % and then decreases steeply for Ni 72 at. %. With further increase in Ni content above 72 at. %, the in-plane H_C again increases.

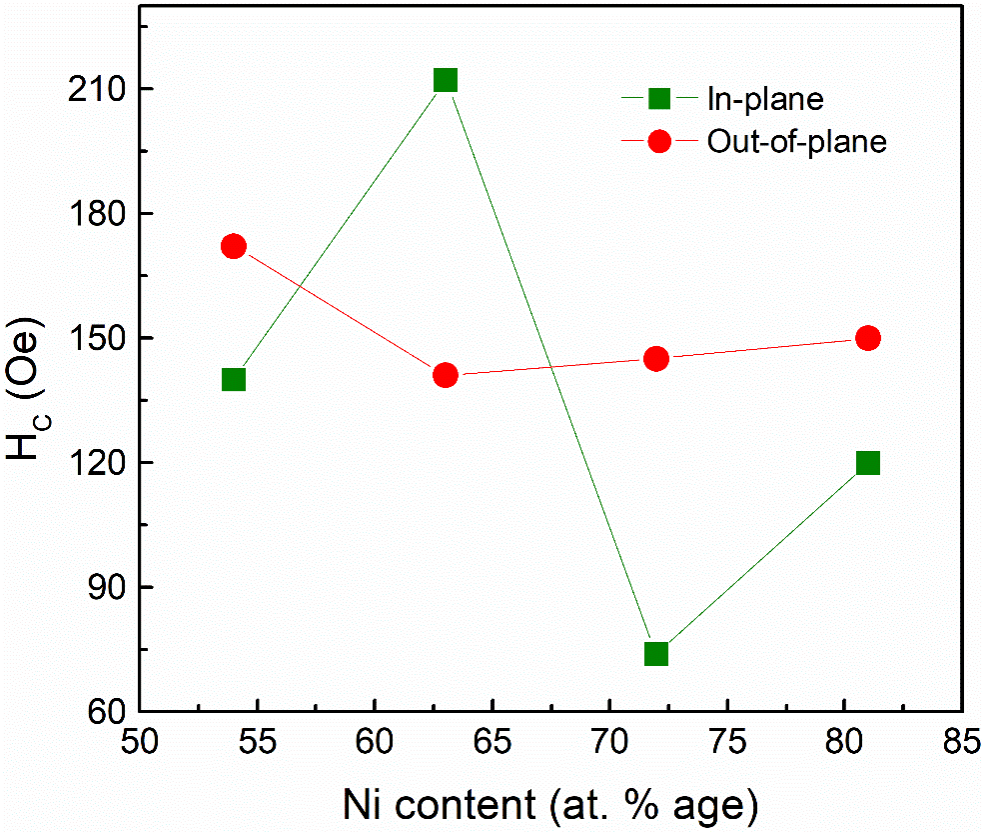

Figure 3.27 Plot of variation of coercive field (H_C) of as-deposited CoTbNi films as a function of Ni-content of the films.

The variation of M_S and M_r of as-deposited films are plotted as a function of Ni content in Figure 3.28. It is seen from Figure 3.28 (a) that the saturation magnetization decreases from 1170 emu/cc to 399 emu/cc with increase in Ni-content. The Ni 54 at. % film has maximum remanent magnetization of 134 and 190 emu/cc for in-plane and out-of-plane direction respectively which decreases

with increase in Ni content to 23 and 43 emu/cc for in-plane and out-of-plane direction respectively. However, the Ni-72 at. % thin film has slightly lower remanence than Ni-81 at. % in In-plane direction. The films also show greater remanence in the perpendicular direction.

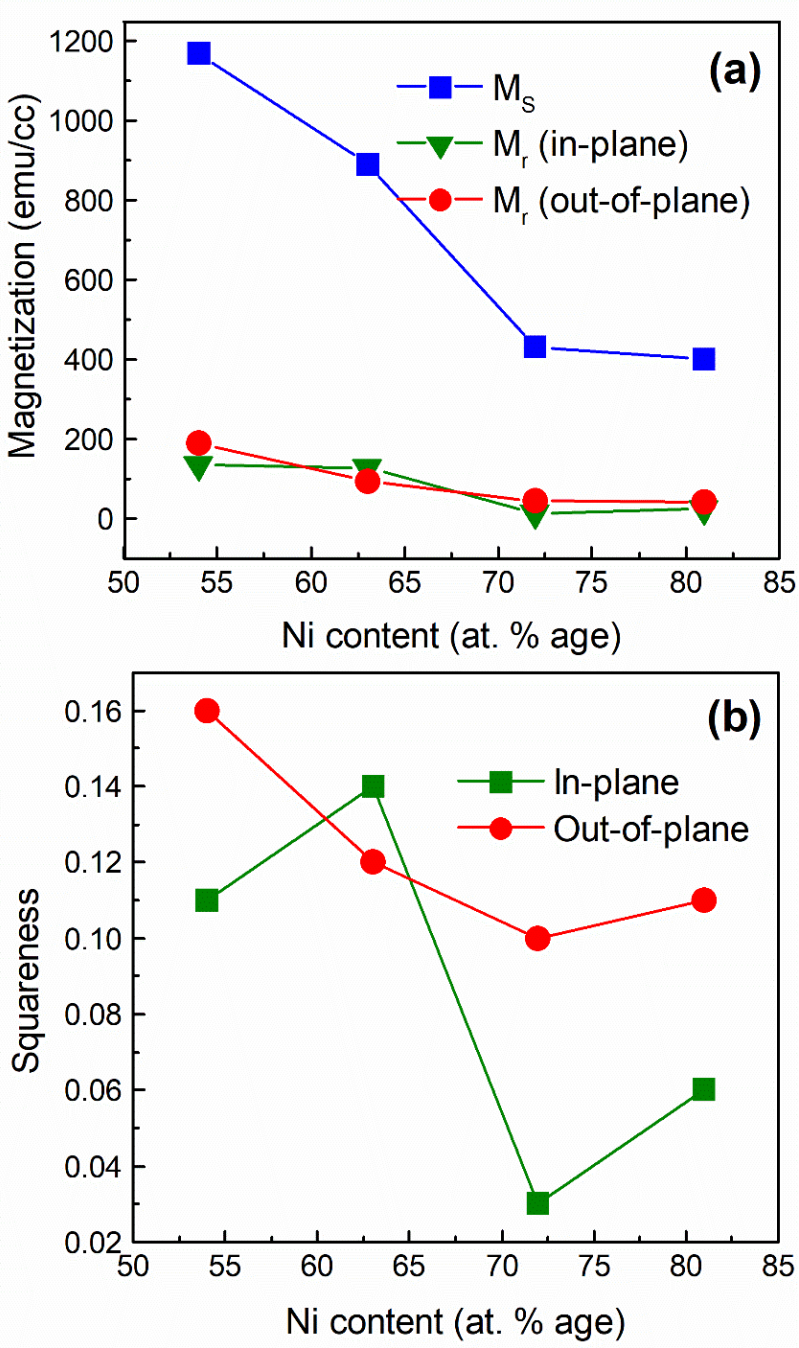

Figure 3.28 Plot of variation of (a) saturation magnetization and remanent magnetization, and (b) squareness as a function of Ni content of as-deposited CoTbNi thin films.

Figure 3.28 (b) shows that the squareness of in-plane magnetization shows an overall decrease with increases in Ni content and the nature of variation is similar to the variation of in-plane coercivity. The Ni 72 at. % exhibit in-plane M-H of smallest squareness. On the other hand, the squareness of out-of-plane M-H loops first decreases with increases in Ni content up to 72 at. % thereafter shows a small increase for Ni 81 at. %. The out-of-plane M-H loops possess better squareness than in-plane M-H loops. The variation of K_{eff} as a function of Ni-content of the samples is plotted in Figure 3.29. The K_{eff} decreases nearly linearly with increase in Ni content of the films. This shows that the addition of Ni to CoTb up to 60 at. % results in magnetic isotropy. Above 60 at. % Ni, the films exhibit PMA. However, the strength of PMA and K_{eff} decreases nearly linearly with increase in Ni content of the films. The decrease in M_S and K_{eff} with Ni addition suggests the antiferromagnetic coupling of Ni with Co as observed in other works [219,220]. Thus addition of Ni to CoTb alloy plays significant role in controlling the magnetic anisotropy in these films.

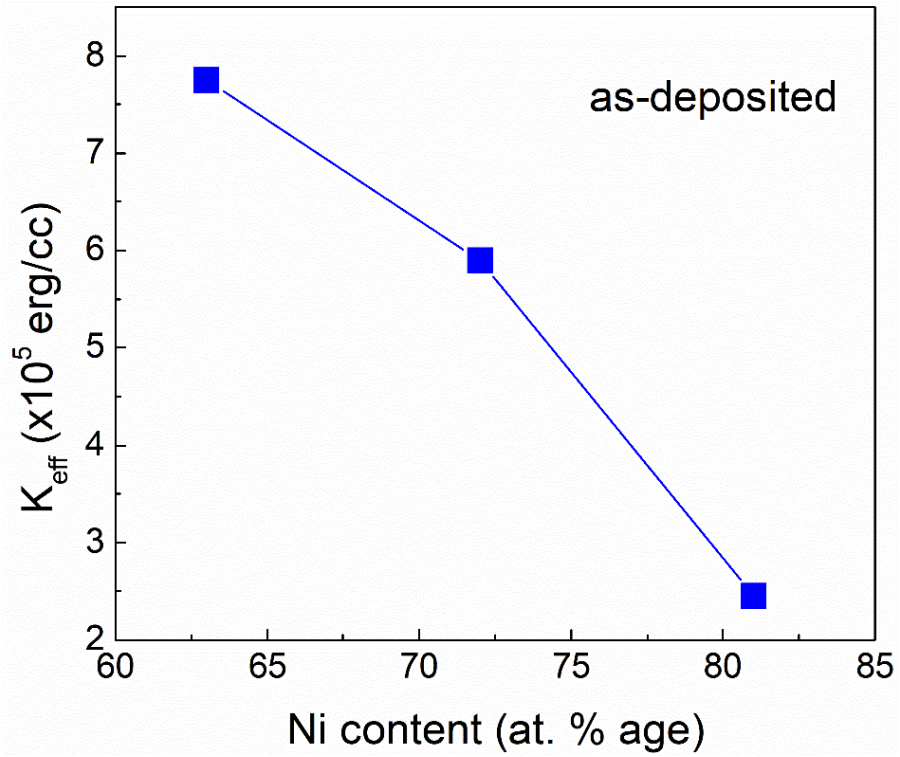

Figure 3.29 Plot of variation of effective anisotropic constant K_{eff} as function of CoTbNi ternary alloy films.

3.6.2 M-T Measurement Results of As-deposited CoTbNi Thin Films

To study the temperature variation of magnetization, the magnetic moment of as-prepared samples were measured as a function of temperature under zero field cooled (ZFC) as well as in field cooled (FC) condition. Generally, the zero-field-cooled (ZFC) magnetization curve is measured during the heating of the sample in the presence of a magnetic field [221–223]. The sample is initially cooled from temperature T_{High} to T_{Low} in absence of magnetic field. In FC process the sample is cooled in the presence of a magnetic field to the temperature T_{Low} and the measurement is performed by increasing the temperature. The FC process is temperature-reversible provided that the temperature rates of cooling process and the reheating process be identical [221,223].

In this thesis, the T_{High} and T_{Low} are chosen as 800℃ (1073K) and room temperature (RT) respectively. Thus in ZFC process, the samples were cooled to room temperature (RT) in absence of magnetic field and then the magnetization was measured in the temperature range from RT to 1073 K under applied field of 500 Oe. In FC process, the samples were cooled to RT under magnetic field then the magnetization was measured under applied field of 500 Oe in the temperature range from RT to 1073 K. The obtained M-T curves are presented in Figure 3.30. It is observed from all FC and ZFC curves that the magnetization does not fall sharply to zero with the increase in temperature. Moreover, the magnetization does falls gradually and is retained to high temperature$\sim 1000\ K$, which suggests that the ferromagnetism is retained up to$\sim 1000\ K$. However, the material does not show sharp transition ferromagnetic regime to a paramagnetic regime at higher temperatures. Due to the absence of this transition, the Curie temperature could not be determined by Curie-Weiss law.

From Figure 3.30 (a), it is observed that magnetization under ZFC condition (M_{ZFC}) of x=0.54 increases continuously from temperature 1073 K to ∼780 K and then slightly drops below this temperature to ∼719 K giving a cusp like signature. Below ∼ 719 K the M_{ZFC} continuously increases. For other samples such a signature has not been observed in ZFC curves (Figure 3.30 (b) and (c)). However, the FC curve

measured for x=0.54 starts diverging from ZFC curve at T~ 822 K. Similar divergence in M_{FC} and M_{ZFC} has been observed in other samples at higher temperatures T ~989 K for x=0.63 and T~917 K for x=0.72 sample. Such divergence of M_{FC} and M_{ZFC} signifies the irreversibility of FC and ZFC curves.

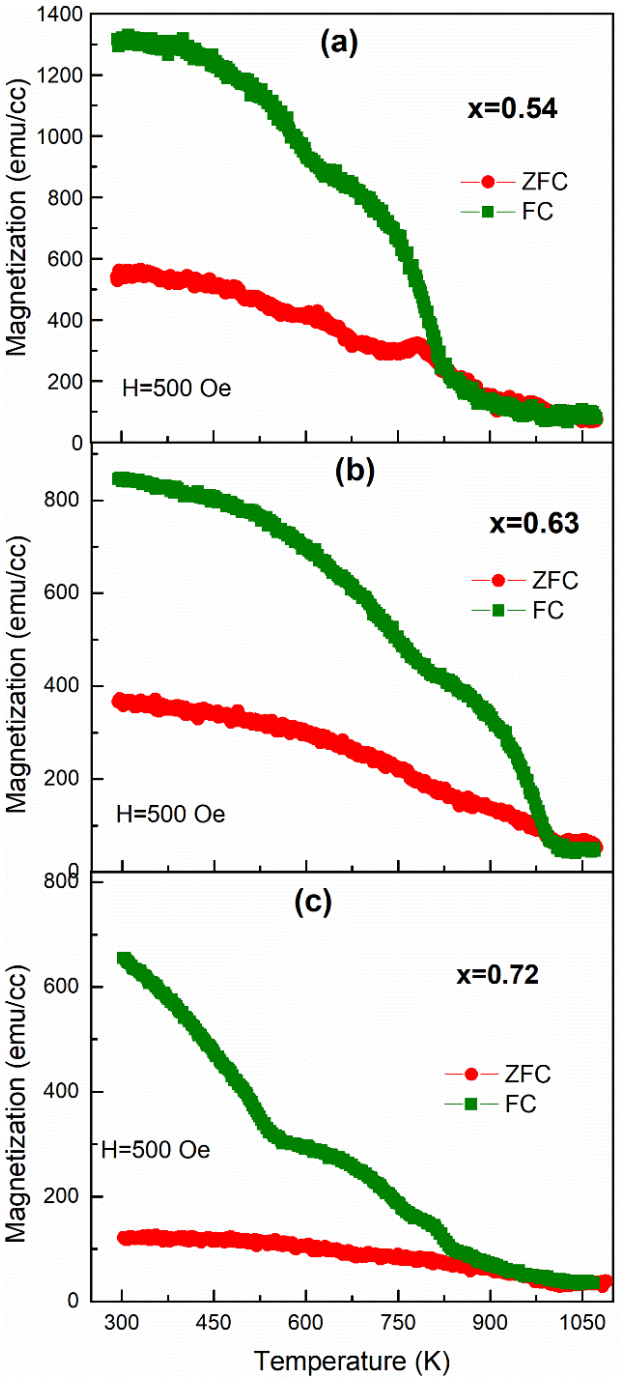

Figure 3.30 Temperature dependent magnetization measurement under zero-field cooled (ZFC) and field-cooled (FC) condition of $(Co_{0.85}Tb_{0.15})_{1-x}Ni_x$ alloy thin films.

In ZFC process, the spins have been locked in arbitrary directions during cooling which gives rise to low magnetization at room temperature. On the other hand, in FC process, the magnetic field is applied during cooling and hence the spins are locked in the direction of applied field. So the net magnetization is found to be greater than that of ZFC process. At low temperatures around 380 K for x=0.54 and 344 K for x=0.63 samples, a sudden change in M_{FC} has been observed. Such change may be due to the presence of some other interactions, the study of which is beyond the scope of the present thesis work. It has also been observed that the difference between M_{FC} and M_{ZFC} for these samples is very large. Such large difference in M_{FC} and M_{ZFC} is the signature of non-collinear magnetic ordering such as sperimagnetism, which usually arises in amorphous Co-Tb films and originated from magnetocrystalline anisotropy [224,225]. The M_{ZFC} of x=0.72 remains relatively constant as compared to x=0.54 and 0.63 but M_{FC} increases from 40 emu/cc at 925 K to ∼660 emu/cc at room temperature. These observations indicate that x=0.72 sample exhibits stronger magnetic anisotropy than x=0.54 and 0.63, which can also be seen in RT M-H curves as discussed in the previous section.

3.6.3 M-H Measurement Results of In-situ Post Annealed CoTbNi Thin Films

The post-annealing of the four CoTbNi films with compositions x=0.26, 0.45, 0.54, and 0.60 has not been carried out as these films exhibit magnetic isotropy. The RT M-H hysteresis loops of $(Co_{0.85}Tb_{0.15})_{0.37}Ni_{0.63}$ are presented in Figure 3.31. The in-plane and out-of-plane magnetization curves saturate at 805 emu/cc at the same applied field of ∼7500 Oe. This shows that this film also exhibits magnetic isotropy in both in-plane and out-of-plane directions. The coercive fields of in-plane and out-of-plane M-H loop are found to be 120 and 145 Oe respectively. The room temperature in-plane and out-of-plane M-H curves of $(Co_{0.85}Tb_{0.15})_{0.28}Ni_{0.72}$ saturate at 970 emu/cc at the same applied field at about 6500 Oe indicating that this film also magnetically isotropic in both the directions as can be seen in Figure 3.32. The obtained RT magnetic parameters are presented in Table 3.8. However, the coercive fields of in-plane and out-of-plane M-H curves of this thin film are found to be different. The coercive fields of in-plane and out-of-plane M-H curves are found to

be 64 Oe and 144 Oe respectively. The out-of-plane M-H curve has a greater remanence of 120 emu/cc than the remanence of 50 emu/cc in the in-plane. Thus out-of-plane M-H curve possesses greater squareness of 0.12 than the in-plane M-H curve of squareness of 0.05. The observed magnetic parameters indicate that this film.

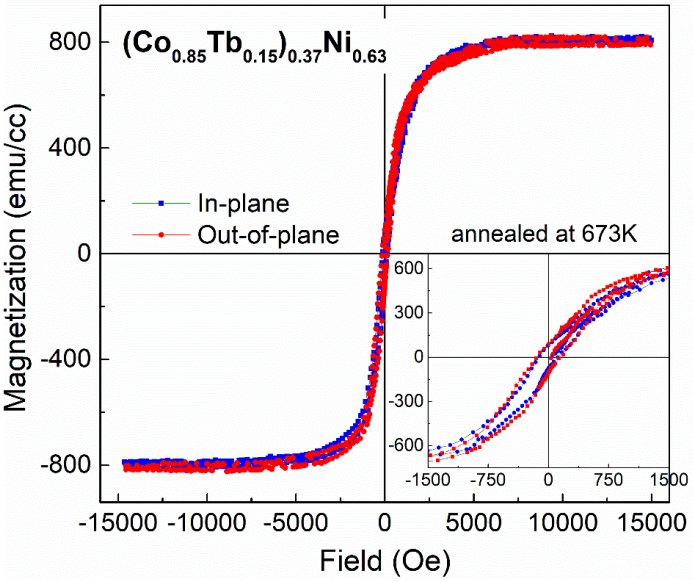

Figure 3.31 Room temperature M-H curve of in-situ post annealed $(Co_{0.85}Tb_{0.15})_{0.37}Ni_{0.63}$ ternary alloy film.

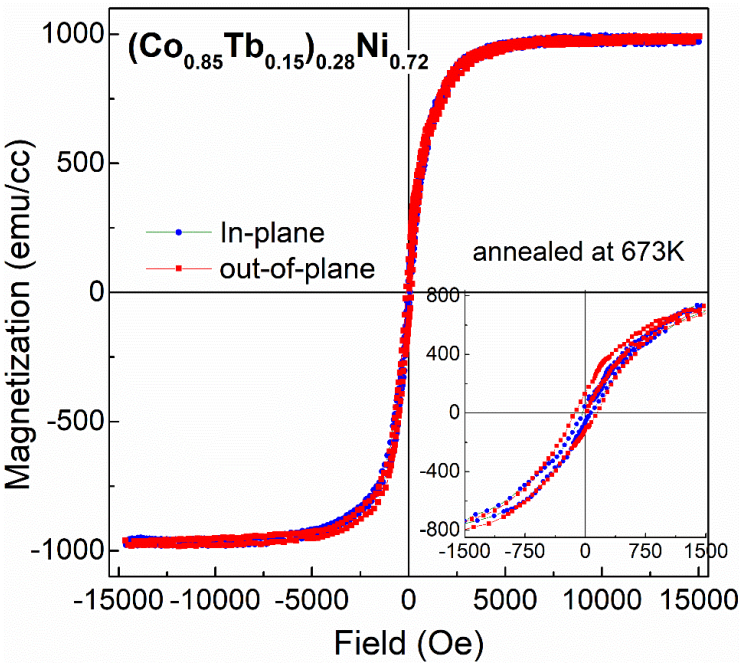

Figure 3.32 Room temperature M-H curve of in-situ post annealed $(Co_{0.85}Tb_{0.15})_{0.28}Ni_{0.72}$ ternary alloy film.

The RT M-H loop of annealed $(Co_{0.85}Tb_{0.15})_{0.19}Ni_{0.81}$ thin film is depicted in Figure 3.33. This film exhibits room temperature ferromagnetism with the smallest saturation magnetization of 368 emu/cc than the other three annealed thin films. Both in-plane and out-of-plane M-H curves saturate at the same applied field of about 7000 Oe, which shows that this film is also magnetically isotropic in both directions. The coercive field of the out-of-plane M-H curve is found to be 150 Oe, which being slightly greater than the coercivity of 125 Oe of in-plane M-H curve. Also the remanent magnetization of out-of-plane M-H curve is found to be 56 emu/cc which is slightly greater than the remanent magnetization of 46 emu/cc of in-plane M-H curve. The out-of-plane M-H curve also exhibits better squareness than the in-plane M-H curve. All the observed magnetic parameters of all in-situ post-annealed thin films have been illustrated in Table 3.8.

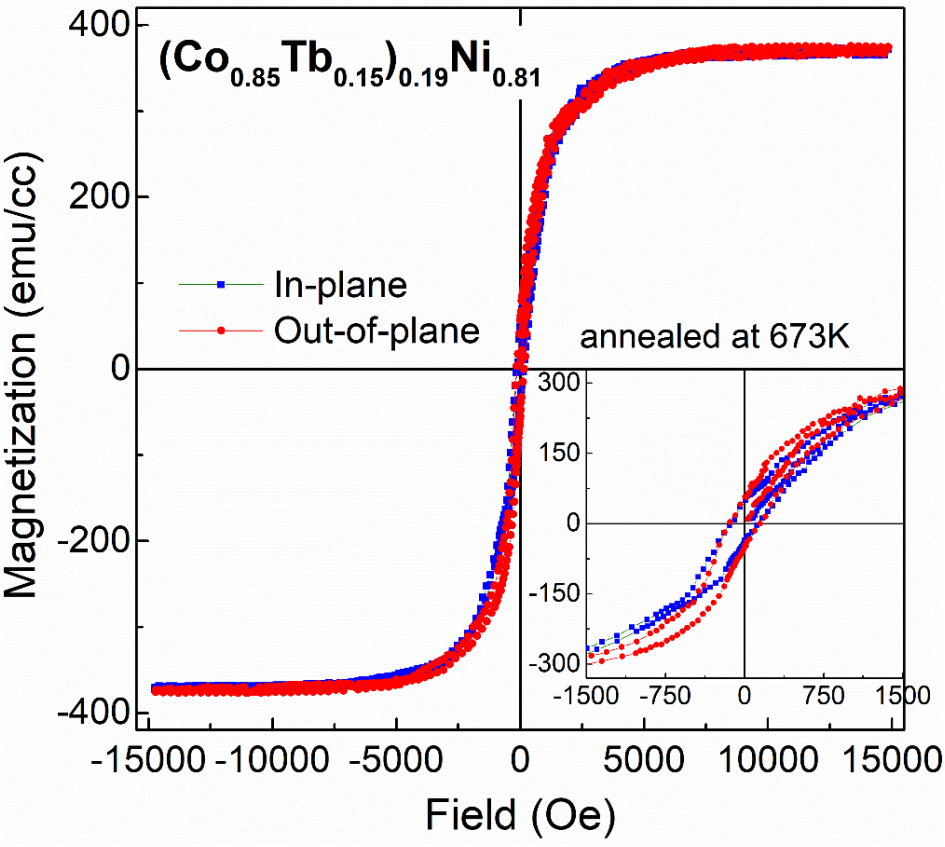

Figure 3.33 Room temperature M-H curve of in-situ post annealed $(Co_{0.85}Tb_{0.15})_{0.19}Ni_{0.91}$ ternary alloy film. The annealing of the film was carried out at 400℃ (673K).

Table 3.8 Magnetic parameters of in-situ post annealed $(Co_{0.85}Tb_{0.15})_{1-x}Ni_x$ ternary alloy thin films obtained from room temperature M-H measurement. The IP and OOP represent in-plane and out-of-plane respectively.

Magnetic Parameters	Samples $(Co_{0.85}Tb_{0.15})_{1-x}Ni_x$					
	x=0.63		x=0.72		x=0.81	
	IP	OOP	IP	OOP	IP	OOP
H_C (Oe)	120	145	64	144	125	150
M_r (emu/cc)	82	91	50	120	46	56
M_S (emu/cc)	805		970		368	
M_r/M_S	0.10	0.11	0.05	0.12	0.12	0.15

To analyze the influence of film compositions on magnetic properties of annealed $(Co_{0.85}Tb_{0.15})_{1-x}Ni_x$ alloy films, the magnetic parameters such as H_C, M_S, M_r, and squareness (M_r/M_S) are plotted as a function of Ni content of the films. From Figure 3.34 it is observed that the in-plane coercive field decreases from 120 Oe for x=0.63 with increase in Ni-content to 64 Oe for x=0.72. Thereafter again increases to 125 Oe for x=0.81 sample. On the other hand, an overall increase in out-of-plane H_C is observed for annealed films. The films possess greater coercivity in out-of-plane direction, which indicates that the hardness increases with an increase in Ni addition. The saturation magnetization also varies nonlinearly with composition of thin films as seen in Figure 3.35. M_S first increases with increase in Ni addition to the CoTb and reaches its peak for x=0.72 film. Further addition of Ni beyond x=0.72 leads M_S to decrease with increase in Ni content. The M_r of out-of-plane M-H curves also varies with Ni content similarly to M_S of the annealed films. However, a steady decrease in in-plane M_r is observed with the increase in Ni content of the films. From Figure 3.36, the nature of variation of squareness (M_r/M_S) of in-plane M-H curves is seen to be similar to the variation of in-plane H_C of the films (Figure 3.34). The in-plane squareness first decreases with Ni content to x=0.72 and thereafter increases with further increase in Ni addition to the CoTb alloy. On the other hand, a steady increase in the squareness of out-of-plane M-H

curves is observed with increase in Ni content of the annealed films. Up to x=0.72 Ni addition, a substantial enhancement of M_S, as well as M_r and squareness of out-of-plane magnetization curves has been observed for annealed films.

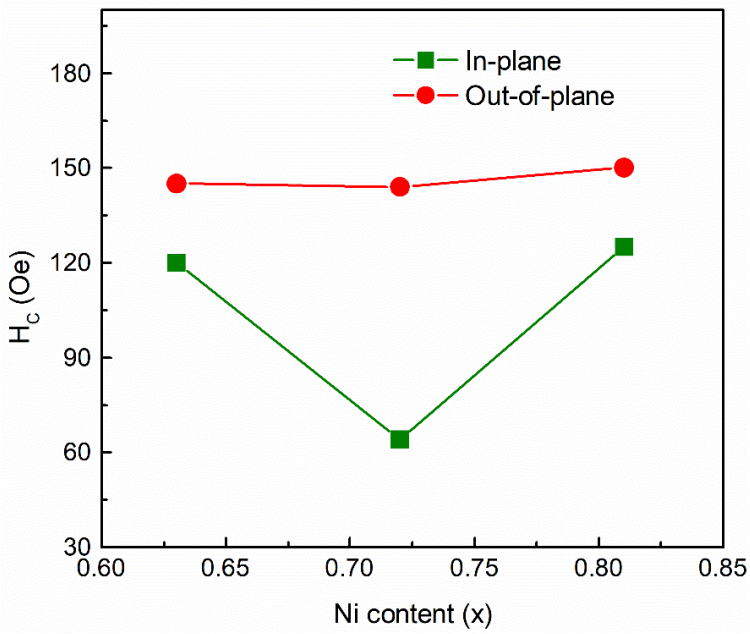

Figure 3.34 Plot of variation of H_C as a function of Ni content of the annealed $(Co_{0.85}Tb_{0.15})_{1-x}Ni_x$ ternary alloy thin films.

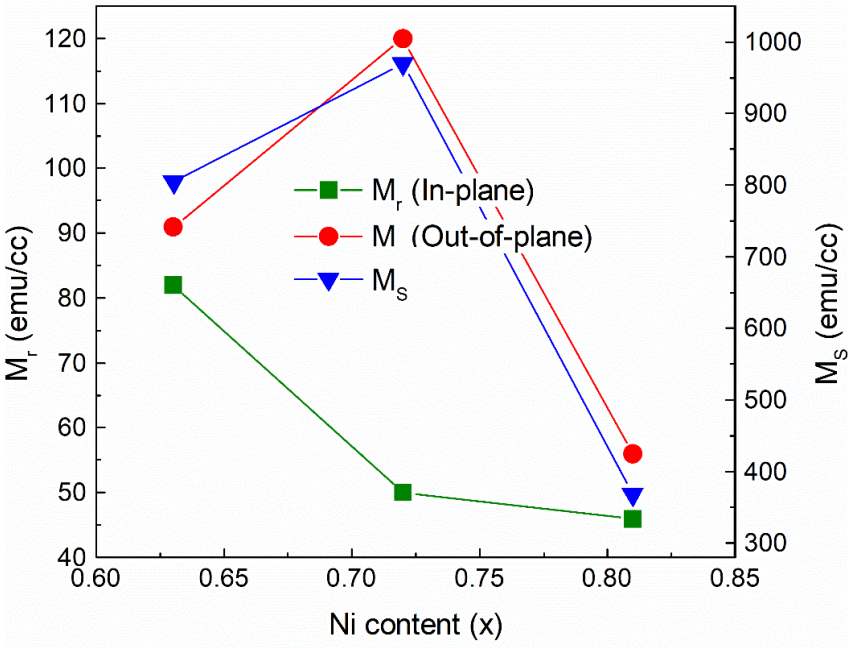

Figure 3.35 Plot of variation of M_r and M_S as a function of Ni content of in-situ post annealed $(Co_{0.85}Tb_{0.15)1-x}Ni_x$ thin films.

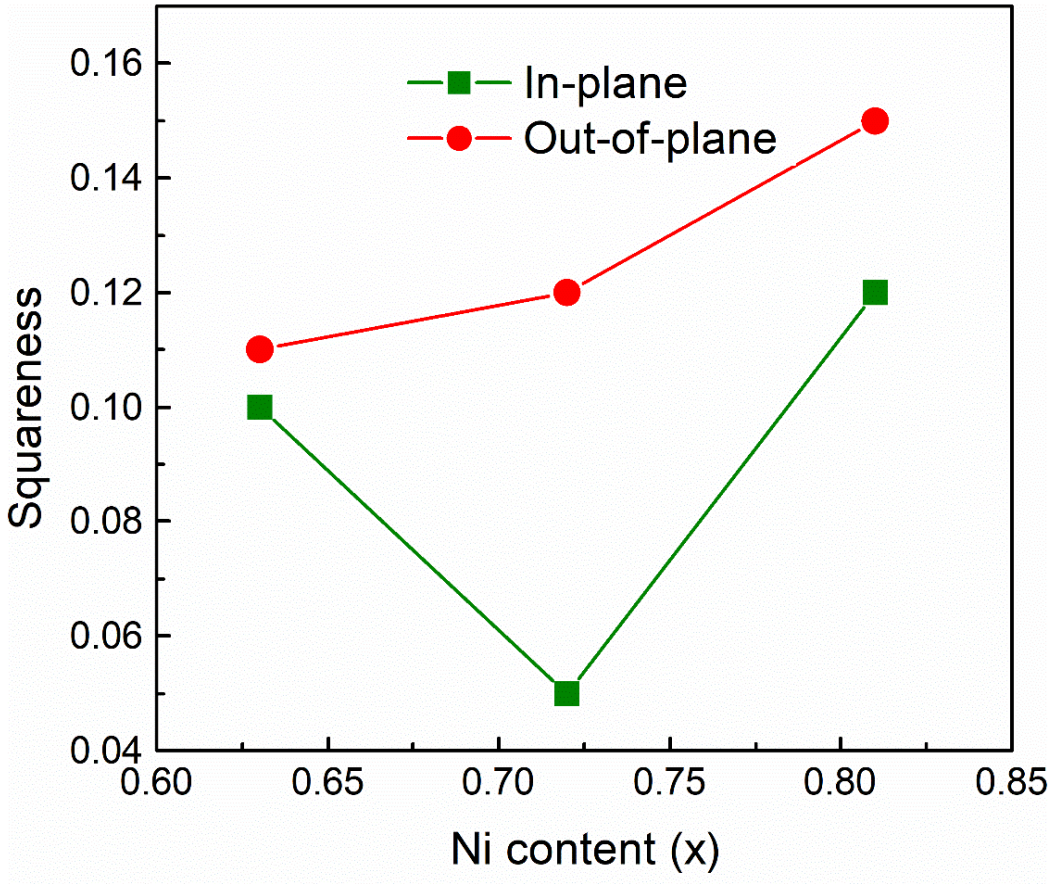

Figure 3.36 Plot of squareness (M_r/M_S) of M-H curves as a function of Ni content of in-situ post annealed $(Co_{0.85}Tb_{0.15})_{1-x}Ni_x$ thin films.

3.6.4 Influence of In-situ Post Annealing on Magnetic Property

The magnetic properties of RE-TM alloy thin films are highly sensitive to a number of parameters such as growth conditions (Ar gas flow rate during deposition [16], substrate choice [10], external strain [13], etc.) and annealing condition of the films [15,226]. Annealing of the sample is one of the vital processes of tuning the magnetic properties of alloy thin films. The magnetic parameters such as coercive field, magnetic moment [14], etc., of the materials are greatly influenced by the annealing temperature of the sample. The annealing of samples at different temperatures also influence the particle size, crystallite size, and morphology of the samples. The magnetic ordering temperatures are also being reported to change with the annealing temperatures and annealing conditions. The annealing process

is carried out for the crystallization of the material, to relieve internal stresses induced during sample fabrication, etc.

Annealing can be done in two ways- one by preheating the substrate to a particular temperature and depositing the sample at that temperature, and the other by slowly heating the deposited sample at the predetermined heating rate to a particular temperature, maintaining at that temperature for a particular duration and then allow it to cool slowly at the predetermined cooling rate to room temperature. In the current thesis work, the deposited films were slowly heated to 673K, maintained at that temperature for one hour, and slowly allowed to cool to room temperature. The entire annealing process was carried out in-situ as soon as the film is deposited and under Ar-gas environment at the same vacuum pressure at which the films were deposited. This annealing process has been termed as in-situ post-annealing.

To analyze the influence of in-situ post-annealing on magnetic properties of CoTbNi alloy films, the obtained magnetic parameters such as H_C, M_S, M_r, and squareness of the all as-deposited and in-situ post annealed films are plotted as a function of Ni content in Figure 3.37 and Figure 3.38. From Figure 3.37 (a), it is seen that the nature of variation of in-plane H_C of annealed films is nearly similar as those of as-deposited films. As-deposited x=0.63 film exhibits the largest in-plane H_C the annealed film and for other films, in-plane H_C is nearly the same. This indicates that the annealing does not influence the in-plane H_C significantly. The as-deposited and post-annealed thin films have nearly the same out-of-plane H_C as it can be seen in Figure 3.37 (b). Figure 3.37 (c) shows that the annealing of the films leads to an overall reduction in M_S, except for x=0.72 film in which an increase in M_S is observed with the annealing of the film. The post-annealing of films influences significantly the M_r of the films. For x=0.63, a reduction in both in-plane and out-of-plane M_r is observed with annealing as indicated in Figure 3.38 (a) and (b). On the other hand, enhanced M_r is observed for annealed x=0.72 and 0.81 films. In Figure 3.38 (c) and (d), a small enhancement is observed in squareness of in-plane M-H loops of x=0.72 and 0.81 films, out-of-plane squareness for x=0.72, and 0.81 upon annealing of the films. Thus annealing of the films is found to play only a little role on the H_C, M_S and M_r of these CoTbNi thin films.

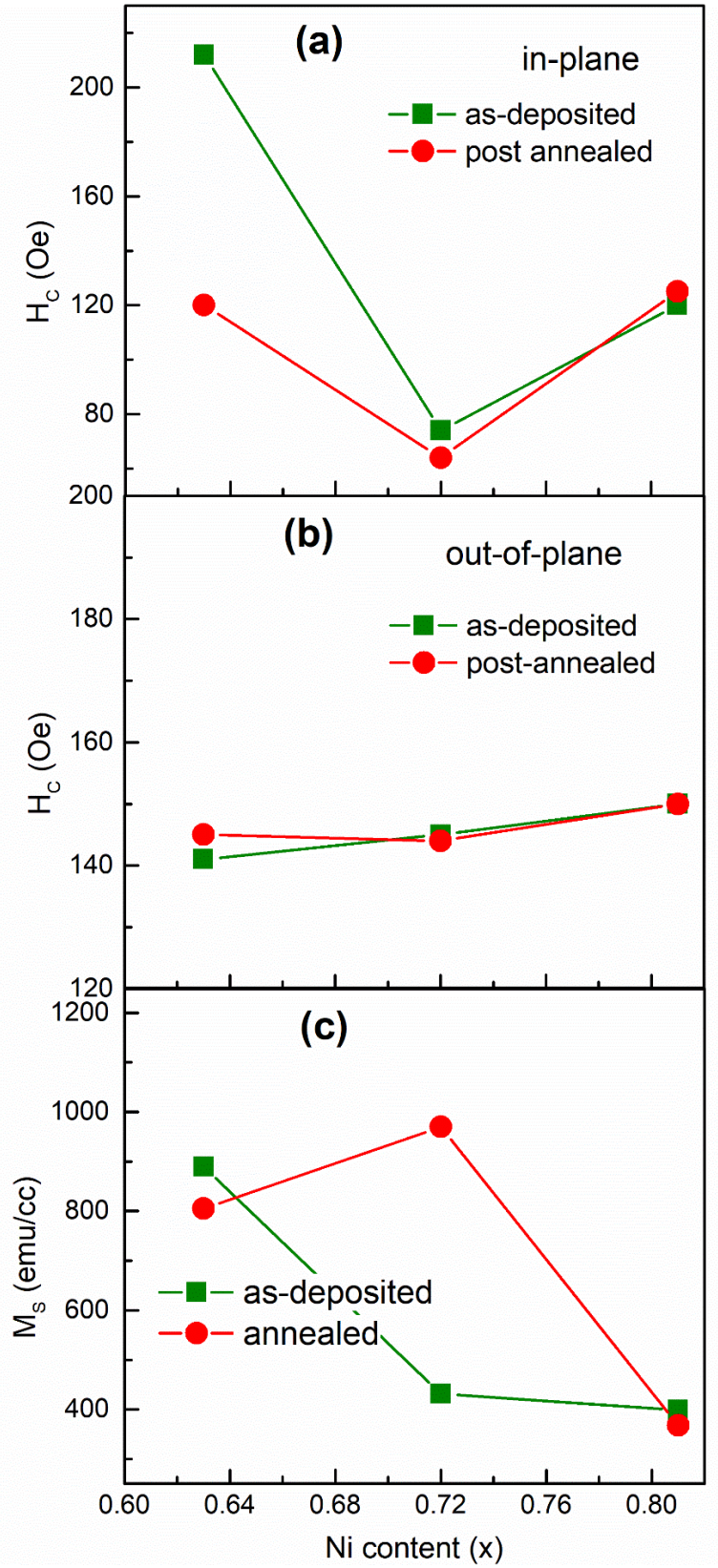

Figure 3.37 Comparative plot of variation H_C and M_S as a function of Ni content of as-deposited and in-situ post annealed $(Co_{0.85}Tb_{0.15})_{1-x}Ni_x$ thin films.

However, the annealing of the films is found to play a significant role in magnetic anisotropy. The PMA observed in as-deposited x=0.63, 0.72, and 0.81 thin films are completely lost due to annealing of the films. This indicates that perpendicular magnetic anisotropy of as-deposited films is changed to magnetic isotropy due to the annealing of the films. A number of suggestions were put forward by several researchers to the possible mechanisms which lead to PMA in the amorphous RE-TM alloy thin films. These include anisotropic pair co-relation [46,227–229], magnetostriction [230], dipolar interaction [45,231], and bond-orientational anisotropy [232]. However, our observation indicates that the PMA in as-deposited materials is likely due to the result of bond-orientational anisotropy (BOA) originating due to the stress developed in the films during the deposition [228,232,233]. The stresses in the samples have been relieved upon annealing of the samples and hence the PMA disappears with annealing. During deposition of the film, the ejected atoms from target material have sufficient energy to be embedded in the film and upon collision with the films, the transfer of momentum and energy of the atom produces localized compressive stress in the film as suggested in [234]. As a result of this, the number of atomic bonds in the compressive direction which is parallel to the plane of the film is greater than that of perpendicular direction. This leads to the formation of local clusters of atoms which then produces long-range strain in the sample. Consequently, the atomic density becomes higher in the plane of film than in perpendicular direction as depicted in the schematic diagram in Figure 3.39. As a result of this, the electronic angular momentum tends to align in perpendicular direction and hence *f*-electrons of Tb favours perpendicular magnetization through spin-orbit coupling. Upon annealing of the film, the atoms might have uniformly redistributed in both the directions thereby strain in the samples are relieved. Thus the uniform atomic distribution in both directions might have favoured isotropic magnetization in the plane as well as in the perpendicular direction. The stress analysis study is beyond the scope of the current thesis work.

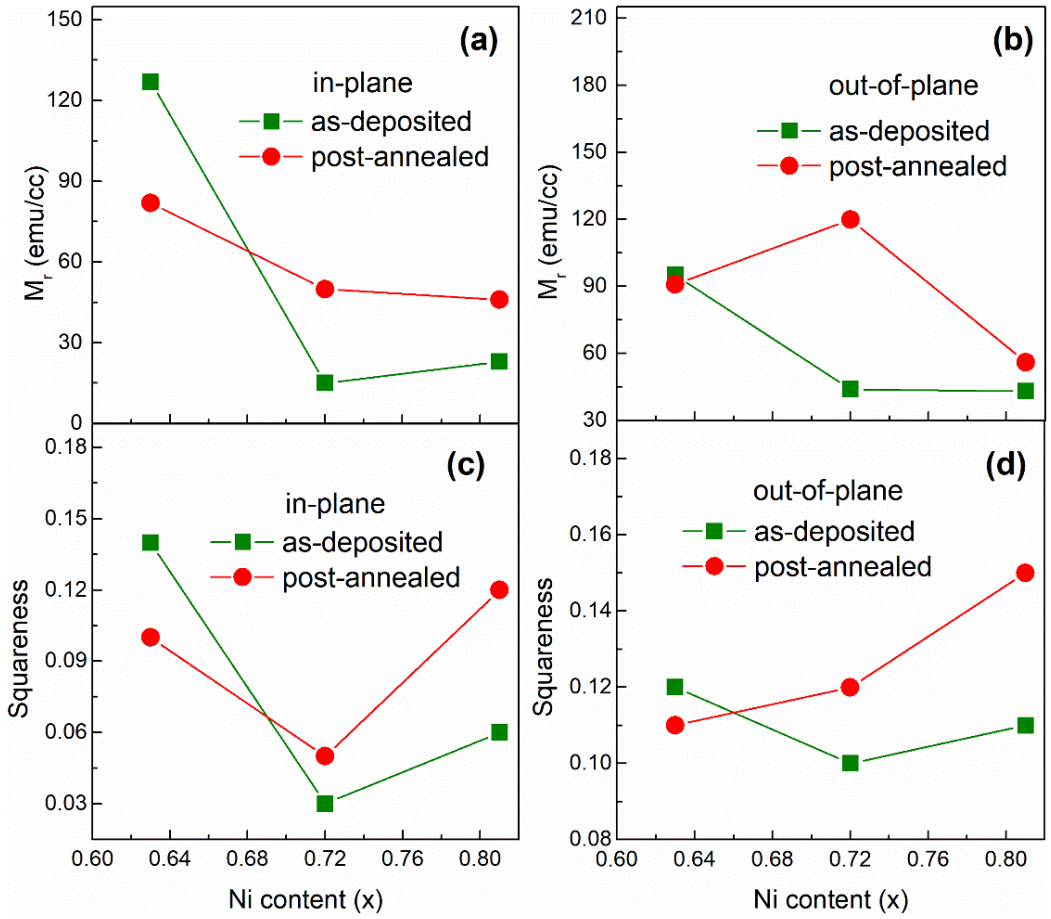

Figure 3.38 Comparative plot of variation M_r and squareness (M_r/M_S) as a function of Ni content of as-deposited and in-situ post annealed $(Co_{0.85}Tb_{0.15})_{1-x}Ni_x$ thin films.

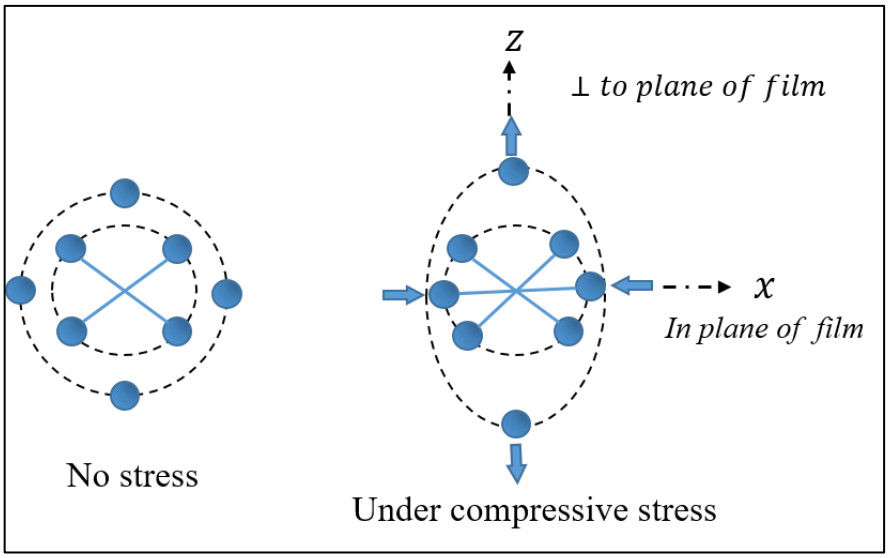

Figure 3.39 A simple example of bond orientation of four atom unit under in plane compressive stress. The solid lines represent atomic bonds.